Cellular/Molecular

Functional Coupling between mGluR1 and $Ca_v3.1$ T-Type Calcium Channels Contributes to Parallel Fiber-Induced Fast Calcium Signaling within Purkinje Cell Dendritic Spines

Michael E. Hildebrand,[1]* Philippe Isope,[2]* Taisuke Miyazaki,[6] Toshitaka Nakaya,[6] Esperanza Garcia,[1] Anne Feltz,[2] Toni Schneider,[5] Jürgen Hescheler,[5] Masanobu Kano,[3] Kenji Sakimura,[4] Masahiko Watanabe,[6] Stéphane Dieudonné,[2] and Terrance P. Snutch[1]

[1]Michael Smith Laboratories, University of British Columbia, Vancouver, British Columbia V6T 1Z4, Canada, [2]Laboratoire de Neurobiologie, Ecole Normale Supérieure, Centre National de la Recherche Scientifique, 75005 Paris, France, [3]Department of Neurophysiology, Graduate School of Medicine, University of Tokyo, Bunkyo-ku, Tokyo 113-0033, Japan, [4]Department of Cellular Neurobiology, Brain Research Institute, Niigata University, Niigata 951-8585, Japan, [5]Institute of Neurophysiology and Center for Molecular Medicine Cologne, University of Cologne, D-50931 Cologne, Germany, and [6]Department of Anatomy, Hokkaido University School of Medicine, Sapporo 060-8638, Japan

T-type voltage-gated calcium channels are expressed in the dendrites of many neurons, although their functional interactions with postsynaptic receptors and contributions to synaptic signaling are not well understood. We combine electrophysiological and ultrafast two-photon calcium imaging to demonstrate that mGluR1 activation potentiates cerebellar Purkinje cell $Ca_v3.1$ T-type currents via a G-protein- and tyrosine-phosphatase-dependent pathway. Immunohistochemical and electron microscopic investigations on wild-type and $Ca_v3.1$ gene knock-out animals show that $Ca_v3.1$ T-type channels are preferentially expressed in Purkinje cell dendritic spines and colocalize with mGluR1s. We further demonstrate that parallel fiber stimulation induces fast subthreshold calcium signaling in dendritic spines and that the synaptic $Ca_v3.1$-mediated calcium transients are potentiated by mGluR1 selectively during bursts of excitatory parallel fiber inputs. Our data identify a new fast calcium signaling pathway in Purkinje cell dendritic spines triggered by short burst of parallel fiber inputs and mediated by T-type calcium channels and mGluR1s.

Introduction

T-type voltage-gated calcium (Ca^{2+}) channels are expressed in a wide range of tissues, including the nervous, cardiovascular, and endocrine systems (Perez-Reyes, 2003). At the molecular level, the T-type Ca^{2+} channel family is composed of three main subtypes ($Ca_v3.1/\alpha_{1G}$, $Ca_v3.2/\alpha_{1H}$, and $Ca_v3.3/\alpha_{1I}$) characterized by similar low thresholds of activation but displaying distinctive expression patterns (Talley et al., 1999; McKay et al., 2006). Recent knockdown studies suggest that individual T-type channel subtypes might play specific physiological roles. In $Ca_v3.1$ knock-out (KO) mice, the typical burst firing mode of thalamic relay cells is absent and defects in sleep behavior are observed (Kim et al., 2001; Anderson et al., 2005), whereas $Ca_v3.2$ KO and knockdown analyses show developmental defects in coronary arteries and pain signaling (Chen et al., 2003; Bourinet et al., 2005).

Recent studies have also demonstrated that T-type channels are functionally expressed in dendritic spines (Carter and Sabatini, 2004; Isope and Murphy, 2005). In cerebellar Purkinje cells (PCs), which reportedly express the $Ca_v3.1$ and $Ca_v3.3$ T-type Ca^{2+} channel isoforms (Talley et al., 1999; Molineux et al., 2006), T-type currents have been associated with dendritic low-threshold spikes and have been shown to control interspike and interburst intervals during spontaneous dendritic burst firing (Pouille et al., 2000; Swensen and Bean, 2003; Womack and Khodakhah, 2004). Although T-type channels are present in PC spines (Isope and Murphy, 2005), their exact contributions to synaptic transmission have not been described.

Isoform-specific T-type Ca^{2+} channel modulation may constitute an important substrate for functional specialization. The $Ca_v3.2$ isoform is regulated by $G\beta_2\gamma$-proteins, CAMKII, and redox changes (Welsby et al., 2003; Wolfe et al., 2003; Joksovic et al., 2006), whereas $G\alpha_{q/11}$-coupled muscarinic acetylcholine receptors (mAChRs) inhibit $Ca_v3.3$ channels but not $Ca_v3.1$ or $Ca_v3.2$ channels (Hildebrand et al., 2007). Hence, T-type channel function may be finely tuned in various cell types according to the combined repertoire of channel isoforms and modulatory pathways. In PC spines, $G\alpha_{q/11}$ is coupled to mGluR1s that are expressed at high levels in dendrites. Activation of mGluR1s by brief parallel fiber (PF) stimulation causes IP_3-mediated local Ca^{2+}

Received Jan. 22, 2009; revised June 12, 2009; accepted June 17, 2009.

This work is supported by an operating grant from the Canadian Institutes of Health Research and a Tier 1 Canada Research Chair in Biotechnology and Genomics-Neurobiology (T.P.S.), by the Centre National pour la Recherche Scientifique, L'Ecole Normale Supérieure, and the L'Agence Nationale pour La Recherche and Human Frontier Science Program, and by Grants-in-Aid for Scientific Research (17023021 and 17100004) from the Ministry of Education, Culture, Sports, Science, and Technology of Japan. M.E.H. was supported by trainee fellowships from the Natural Sciences and Engineering Research Council of Canada and Michael Smith Foundation for Health Research. We thank Drs. Brian MacVicar, Boris Barbour, and Clement Léna for suggestions and comments. We thank Neuromed Pharmaceuticals for kindly providing HEK 293 cell lines stably expressing rat brain $Ca_v3.1$, $Ca_v3.2$, or $Ca_v3.3$ subunits.

*M.E.H. and P.I. contributed equally to this work.

Correspondence should be addressed to Dr. Terrance P. Snutch, Michael Smith Laboratories, University of British Columbia, 2185 East Mall, Vancouver, BC V6T 1Z4, Canada. E-mail: snutch@msl.ubc.ca.

DOI:10.1523/JNEUROSCI.0362-09.2009

 0270-6474/09/299668-15$15.00/0

release in spines (Finch and Augustine, 1998; Takechi et al., 1998) and the activation of a slow EPSC (sEPSC) (Staub et al., 1992; Batchelor et al., 1997; Tempia et al., 2001). The activation of mGluR1s plays a central role in the induction of long-term plasticity at the PF synapse and controls cerebellar motor learning (Aiba et al., 1994; Conquet et al., 1994; Ichise et al., 2000).

We set out to study the interactions between mGluR1s and T-type channels in PCs from rodents. We find that mGluR1 activation selectively potentiates the $Ca_v3.1$ T-type channels within PC proximal dendrites and spines. The mGluR1-mediated potentiation of $Ca_v3.1$ channels occurs through a G-protein- and protein tyrosine-phosphatase-dependent pathway that can be triggered by trains of PF stimulation and is effective after two or three stimulations. These data present the first evidence for a spine-level synergy between T-type Ca^{2+} channel activation and mGluR1-mediated signaling in response to bursts of synaptic transmission.

Materials and Methods

HEK 293 cell culture, transfection, and electrophysiology. All equipment, procedures, and reagents were used as described in detail for the similar study of modulation of recombinant T-type channels by muscarinic acetylcholine receptors (Hildebrand et al., 2007). Briefly, HEK 293 cells that stably expressed rat $Ca_v3.1$, $Ca_v3.2$, or $Ca_v3.3$ subunits were transiently transfected with mGluR1a using Lipofectamine (Invitrogen), and perforated patch recordings (with β-Escin) were performed 48 h later. The external recording solution contained the following (in mM): 2 $CaCl_2$, 1 $MgCl_2$, 10 HEPES, 40 tetraethylammonium (TEA)-Cl, 92 CsCl, and 10 glucose, pH 7.4. The internal pipette solution contained the following: 120 mM Cs-methanesulfonate, 11 mM EGTA, 10 mM HEPES, 2 mM $MgCl_2$, and 75–100 μM β-Escin, pH 7.2. During pharmacology experiments, cells were considered "potentiated" or "inhibited" when they displayed a >10% modulating effect with a clear exponential time course. All remaining cells were grouped into a "no effect" group. To quantify the effect of 100 μM glutamate, peak current levels were allowed to reach equilibrium, and then two to five values were averaged. We note that a subset of cells for all three T-type isoforms showed no modulation by mGluR1a application, which might be explained by a lack of functional expression of mGluR1a in some transfected cells and/or the heterogeneous efficacy of the downstream signaling cascade.

Animals. All experimental procedures involving animals and their care were performed in accordance with the recommendations of the Canadian Council on Animal Care and were according to the animal care regulations and policies of the University of British Columbia, the Centre National de la Recherche Scientifique, and the Hokkaido University School of Medicine. Mice lacking the *cacna1e* gene (encoding $Ca_v2.3$) and the *cacna1g* were, respectively, produced as described previously (Pereverzev et al., 2002; Petrenko et al., 2007). All animals were bred under an identical C57BL/6 background and littermate controls were used when possible. When littermates could not be used, the control animals were age matched to the knock-out animals for the given experiment.

Slice preparation for young rats. Experiments shown in Figures 1, 2 (excluding *E* and *F*), 3, and 6 were performed on male Wistar rats (8–12 d old). Animals were anesthetized with halothane and decapitated, the head was immediately chilled over ice, and the cerebellar vermis was removed with a scalpel and placed in ice cold bicarbonate-buffered saline (BBS) solution containing the following (in mM): 120 NaCl, 3 KCl, 26 $NaHCO_3$, 1.25 NaH_2PO_4, 2 $CaCl_2$, 1 $MgCl_2$, 20 glucose, 1 kynurenate, and 0.1 picrotoxin. During cutting, incubating, and recording, slices were constantly bubbled with 95% O_2/5% CO_2 (carbogen). The vermis was glued in the sagittal orientation to the stage of a Vibratome 1500 Sectioning System, and 200–250 μm sagittal slices were cut from the cerebellar vermis, transferred to BBS at 32°C, and allowed to cool down passively to room temperature.

Slice preparation for mice. The experiments of Figure 2, *E* and *F*, were performed on CBL57/BL6 mice between postnatal day 8 (P8) and P12 and the experiments of Figures 7 and 8 on CBL57/BL6 mice between P15 and P25. Slices were cut in a protecting solution containing the following (in mM): 130 K-gluconate, 14.6 KCl, 2 EGTA, 20 HEPES, 25 glucose, 0.05 D-APV, and 0.00005 minocycline. Before the transfer into normal BBS solution, slices were soaked in sucrose-based solution containing the following (in mM): 230 sucrose, 2.5 KCl, 26 $NaHCO_3$, 1.25 $NaHPO_4$, 25 glucose, 0.8 $CaCl_2$, 8 $MgCl_2$, 0.05 D-APV, and 0.00005 minocycline.

Electrophysiological recordings (animals between P8 and P12). For T-type Ca^{2+} current measurements, mouse or rat cerebellar slices were transferred to a recording chamber and perfused with bubbling modified BBS external solution containing the following (in mM): 120 NaCl, 3 KCl, 26 $NaHCO_3$, 1.25 NaH_2PO_4, 2 $CaCl_2$, 1 $MgCl_2$, 20 glucose, 1 kynurenate, 0.1 picrotoxin, 0.3 tetrodotoxin, 5 TEA-Cl, 1 4-aminopyridine, 0.05 $NiCl_2$, and 0.02 $CdCl_2$. The 20 μM Cd^{2+} was used as an effective antagonist of all high voltage-activated (HVA) Ca^{2+} currents that left T-type currents unaffected (Tai et al., 2006), whereas 50 μM Ni^{2+} blocked R-type but not $Ca_v3.1$ or $Ca_v3.3$ currents (Zamponi et al., 1996; Lee et al., 1999). Cerebellar PCs were visually identified using a Zeiss Axioskop 2 or an Olympus BX51 microscope. Whole-cell patch-clamp recordings from PCs were performed using a Multiclamp 700B amplifier or an Axoclamp 2B, digitized at 2 kHz (Digidata 1322A; MDS Analytical Technologies) and controlled and monitored with a computer running pClamp9 software (MDS Analytical Technologies). Patch pipettes (borosilicate glass BF150-86-10; Sutter Instruments) were pulled using a Sutter P-87 puller and had typical resistances of 3–5 MΩ when filled with internal solution.

For voltage-clamp experiments, the internal solution contained the following (in mM): 140 cesium methanesulfonate, 5 TEA-Cl, 0.5 $MgCl_2$, 10 HEPES, 4 MgATP, 0.5 Na_3GTP, and 0.3 EGTA, adjusted to pH 7.3 (~290 mOsm). In specific pharmacology experiments, 0.5 mM Na_3GTP was replaced with 2 mM guanosine-5′-*O*-(2-thiodiphosphate) (GDP-β-S). To ensure the quality of the space clamp, modulatory effects were studied on T-type currents of moderate amplitude (213 ± 35 pA; $n = 19$) elicited every 10 s from a holding potential of −75 mV (with a 500 ms prepulse to −90 mV to remove inactivation) and depolarizing test pulses ranging between −50 and −35 mV. Cells with leak current (voltage-clamped baseline currents recorded from the holding potential period) above 600 pA at $V_h = -75$ mV were discarded. Data were low-pass filtered at 2 kHz using the built-in Bessel filter of the amplifier, with sampling at 20 kHz. Series resistance was compensated between 70 and 80% on every cell, whereas liquid junction potentials that were calculated to be ~9 mV (at 22°C) were left uncorrected. Leak subtraction of capacitance and leakage current was performed online using a P/6 protocol with reverse polarity pulses for channel kinetics experiments and with Clampfit9 (MDS Analytical Technologies) during offline analysis for all other experiments. Current–voltage relationships and channel activation and inactivation kinetics were analyzed as described previously (Hildebrand et al., 2007). All voltage-clamp recordings were performed at room temperature (20–24°C) except for the subset of experiments shown in supplemental Figure 1 (available at www.jneurosci.org as supplemental material) (31°C). Figures and fittings used the software program Microcal Origin and Illustrator CS2 (Adobe Systems). Analyses were performed using Igor Pro software (WaveMetrics). Statistical significance was determined by Student's *t* tests or nonparametric Wilcoxon's rank tests, and significant values were set as indicated in the text and figure legends.

Combined electrophysiological recordings and ultrafast two-photon calcium imaging. Whole-cell recordings in young rats (P8–P12) (see Fig. 6) were performed using the same solutions, at room temperature, as described above. Slices were preincubated for at least 30 min in a chamber containing 1 ml of BBS supplemented with 1 μM Agatoxin IVA/0.1% BSA to block P/Q-type Ca^{2+} channels. Parallel fiber experiments (see Figs. 7, 8) were performed on P15–P25 mice at 32°C in current-clamp mode using an internal solution containing the following (in mM): 135 $KMeSO_4$, 6 NaCl, 1 $MgCl_2$, 10 HEPES, 4 MgATP, and 0.4 Na_2GTP adjusted to pH 7.3 [~290 mOsm supplemented with 10–20 μM Alexa 594 (Invitrogen) and 400 μM Fluo5F]. The liquid junction potential was calculated to be ~9 mV (at 32°C) for these solutions and was left

uncorrected. PC imaging was started after at least 30 min of whole-cell dialysis.

Calcium transients in PCs were imaged with a custom-built multiphoton laser scanning microscope (for a detailed description, see Otsu et al., 2008) in which both X and Y scanning are operated by acousto-optic deflectors (AODs) (based on the AA.DTS.XY-250 model; A-A Opto-Electronics). Two-photon excitation was produced by an infrared titanium–sapphire pulsed laser (Tsunami pumped by a Millenia VI; Spectra Physics) set to 825 nm and tuned to 700 fs to mitigate AOD-induced dispersion. In this nonmechanical scanning microscope, deflection of the laser beam to a specific position is obtained by setting the appropriate acoustic wavelength in the AOD crystal. Switching the illumination between any two points takes 4 μs, permitting random access imaging at high frame rates. National Instruments boards programmed under Labview were used to implement digital scanning strategies and to synchronize AOD scanning and photon-counting detection with a cooled AsGaP photomultiplier (H7421-40; Hamamatsu).

Spines were resolved and points of interest (POIs) were placed on spine heads and attached dendritic shafts. Optical transients were subsequently monitored simultaneously in 10–50 spines and dendrites at frame rates close to 1 kHz (dwell time, 20–50 μs). In this multiunit recording mode, the POIs sequence is sampled repetitively, and the signal for each location is displayed online as a continuous or episodic recording and analyzed offline using custom routines written in Igor (WaveMetrics). Variation of fluorescence was calculated as a ratio of the change in fluorescence (ΔF) of the Ca^{2+} dye in a 100 ms time window around the peak Ca^{2+} transient and compared with baseline over the fluorescence (R) of the red dye (Alexa 594), labeled $\Delta F/R$. This ratiometric strategy overcomes movements and errors attributable to changes in basal Ca^{2+} or dye concentration. However, it should be noted that this $\Delta F/R$ scaling method precludes direct comparisons of specific values between instruments or laboratories.

Compounds and perfusion. (*S*)-3,5-Dihydroxyphenylglycine (DHPG), LY367385 [(*S*)-(+)-α-amino-4-carboxy-2-methylbenzeneacetic acid], MCPG [(*S*)-α-methyl-4-carboxyphenylglycine], U73122 (1-[6[[(17β)-3-methoxyestra-1,3,5(10)-trien-17-yl]amino]hexyl]-1*H*-pyrrole-2,5-dione), IEM 1460 (*N*,*N*,*N*-trimethyl-5-[(tricyclo[3.3.1.13,7]dec-1-ylmethyl)amino]-1-pentanaminium bromide hydrobromide), SKF 96365 [1–2-(4-methoxyphenyl)-2-[3-(4-methoxyphenyl)propoxy]ethyl-1*H*-imidazole], JNJ16259685 (JNJ), PP1 [1-(1,1-dimethylethyl)-1-(4-methylphenyl)-1*H*-pyrazolo[3,4-d]pyrimidin-4-amine], and PP2 [3-(4-chlorophenyl) 1-(1,1-dimethylethyl)-1*H*-pyrazolo[3,4-d]pyrimidin-4-amine] were all obtained from Tocris Bioscience. Edelfosine and bpV(phen) were obtained from Calbiochem. All other drugs were ordered from Sigma-Aldrich. Drugs were dissolved in dH_2O, equimolar NaOH, or DMSO, according to the solubility data of the manufacturer. The highest concentration of DMSO in the extracellular or intracellular solutions did not exceed 0.1%, a concentration that did not detectably affect Ca^{2+} channel properties. A closed perfusion system (5–20 ml) was also used to maintain high concentrations of antagonists and agonists during experiments. In experiments aimed at a more physiological activation of mGluR1, DHPG was puffed directly onto the recorded PC using a 50 ms, 10 psi pressure pulse delivered by a Parker Hannifin Picospritzer III to a patch pipette loaded with 100 μM DHPG and placed within close proximity of the PC. Control recordings showed that puffing on antagonist was able to block T-type currents [puffing 100 μM SKF 96365 inhibited T-type current by 28 ± 4% ($n = 4$), whereas puffing control BBS had no effect on T-type currents (2 ± 1%; $n = 2$)].

Immunohistochemistry. The primary antibodies used here are listed in supplemental Table 2 (available at www.jneurosci.org as supplemental material). In this study, we produced a guinea pig polyclonal antibody to the C-terminal sequence of mouse $Ca_v3.1$ using a synthetic peptide (CPKKDALSLSGLSSDP) conjugated to keyhole limpet hemocyanin. All immunohistochemical incubations were done at room temperature in a free-floating state. For immunofluorescence, microslicer sections were incubated with 10% normal donkey serum for 20 min, primary antibodies overnight (1 μg/ml or 1:10,000 dilution), and Alexa Fluor-488- or indocarbocyanine-labeled species-specific secondary antibodies for 2 h (1:200; Invitrogen and Jackson ImmunoResearch). PBS-containing 0.1% Tween 20 was used for the dilution of antibodies and the washing buffer. Images were taken with a dissecting microscope (AX-70; Olympus) equipped with a digital camera (DP70; Olympus) or with a confocal laser scanning microscope (FV1000; Olympus). Methods for preembedding and postembedding immunogold electron microscopy were described previously (Tanaka et al., 2000), and electron micrographs were taken with an H-7100 electron microscope (Hitachi).

Results

mGluR1 activation differentially modulates T-type Ca^{2+} channels

Because available pharmacological tools do not allow for discrimination among native T-type channel isoforms, potential functional interactions between mGluR1s and T-type channels were initially analyzed in HEK 293 cell lines stably expressing individual recombinant rat brain T-type isoforms and then transiently transfected with mGluR1a (Fig. 1). Activation of mGluR1a with 100 μM glutamate caused a potentiation of $Ca_v3.1$ and $Ca_v3.2$ currents and an inhibition of $Ca_v3.3$ currents (Fig. 1). Compared with the rapid onset inhibition of the $Ca_v3.3$ currents ($\tau_{onset} = 16 \pm 2$ s, $n = 14$), the time course of the potentiation of $Ca_v3.1$ and $Ca_v3.2$ currents was relatively slow ($Ca_v3.1$, $\tau_{onset} = 95 \pm 15$ s, $n = 6$; $Ca_v3.2$, $\tau_{onset} = 225 \pm 22$ s, $n = 5$) and included a "lag" period, suggesting that the intracellular pathway(s) mediating the two effects might be different (Fig. 1). Furthermore, $Ca_v3.1$ and $Ca_v3.2$ current kinetics were not significantly ($p > 0.05$) affected during the mGluR1a-induced potentiation, whereas the inhibition of $Ca_v3.3$ by mGluR1a was accompanied by a significant speeding of activation and inactivation (Fig. 1) (for $Ca_v3.3$: control, $\tau_{act} = 6.4 \pm 0.4$ ms, $n = 25$, $\tau_{inact} = 76 \pm 8$ ms, $n = 13$; 100 μM glutamate, $\tau_{act} = 4.4 \pm 0.3$ ms, $n = 25$, $\tau_{inact} = 39 \pm 5$ ms, $n = 13$; $p < 0.02$). It should be noted that, in a subset of cells, the mGluR1a-mediated inhibition of $Ca_v3.3$ currents was followed by a slower recovery and/or stimulation (data not shown), indicating that, under some circumstances, $Ca_v3.3$ channels may be stimulated by mGluR1a. Together, the results show the differential mGluR1-mediated modulation of T-type currents in a heterologous system.

$Ca_v3.1$ T-type Ca^{2+} currents are potentiated by mGluR1 activation in young cerebellar Purkinje neurons

To investigate the mGluR1-mediated T-type Ca^{2+} channel modulation in a more native system, we first recorded isolated whole-cell T-type currents in juvenile PCs (P8–P12) from rat cerebellum as described previously (Isope and Murphy, 2005) (see Materials and Methods) (Fig. 2). At this age, mGluR1 and T-type currents are both expressed (Shigemoto et al., 1992; Isope and Murphy, 2005), whereas the dendritic arbor is small enough to alleviate space-clamp problems (Roth and Hausser, 2001; Sacco and Tempia, 2002). Depolarizing steps from a holding potential of −90 mV can evoke inward T-type currents that exceed 1 nA (data not shown). Thus, modulatory effects were studied on submaximal T-type currents of moderate amplitude (213 ± 35 pA, $n = 19$; depolarizing steps between −50 and −35 mV) (Figs. 2, 3) (see also Fig. 6) to reduce voltage-clamp escape in the dendrites. Activation of mGluR1s by bath application of DHPG (20 μM) caused a robust and reversible increase in T-type peak current amplitude in all PCs tested (51 ± 7%, $n = 19$, $p < 0.02$; reversed by 84 ± 11%, $n = 5$) (Fig. 2*A*, *B*, *D*). The DHPG-induced potentiation of T-type currents did not involve a significant change in the activation (τ_{act}) or inactivation (τ_{inact}) kinetics of the current (Fig. 2*A*) (supplemental Table 1, available at www.jneurosci.org as supplemental material). The increase in T-type

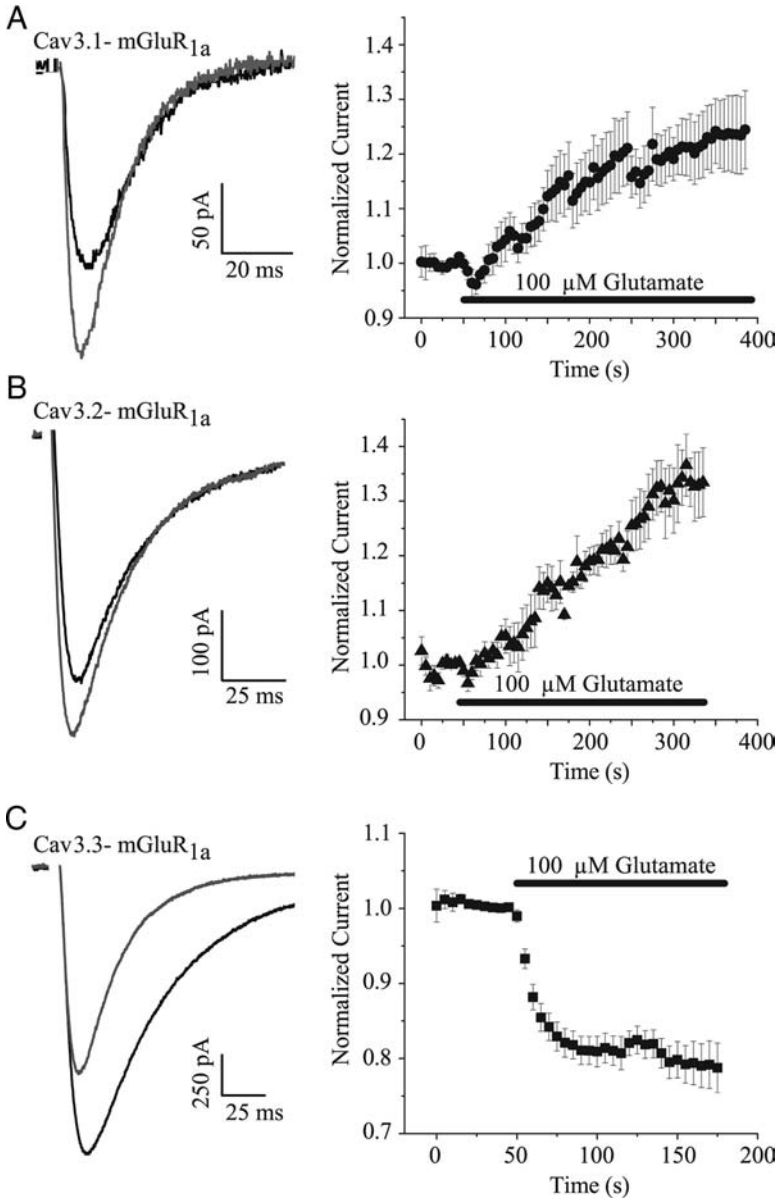

Figure 1. mGluR1 differentially modulates T-type Ca^{2+} channels. ***A–C***, Left, Representative voltage-clamped current traces during depolarizing pulses from −110 to −30 mV (or −40 mV for ***C***) in HEK 293 cells coexpressing recombinant mGluR1a and the indicated T-type isoform. Activation of mGluR1a with 100 μM glutamate (gray line) caused a potentiation of $Ca_v3.1$ (***A***) and $Ca_v3.2$ (***B***) currents and an inhibition of $Ca_v3.3$ (***C***) currents. Right, Normalized peak current levels during perfusion of control recording solution (2 mM Ca^{2+}), followed by 100 μM glutamate for $Ca_v3.1$ (***A***), $Ca_v3.2$ (***B***), and $Ca_v3.3$ (***C***) currents. The potentiation shown for $Ca_v3.1$ and $Ca_v3.2$ channels was observed in ~30% of cells tested, whereas the mGluR1a-induced inhibition of $Ca_v3.3$ currents was observed in ~70% of cells. mGluR1a activation caused an average potentiation (at equilibrium for each cell; see Materials and Methods) of $Ca_v3.1$ currents by 29.6 ± 5.8% ($n = 8$), potentiation of $Ca_v3.2$ currents by 41.8 ± 8.8% ($n = 6$), and inhibition of $Ca_v3.3$ currents by 28.7 ± 1.9% ($n = 33$). For $Ca_v3.1$ and $Ca_v3.2$ currents, glutamate had no effect on all excluded cells, whereas for $Ca_v3.3$, 100 μM glutamate caused either no effect or inhibition followed by a stimulation/recovery in the cells not shown (data not shown; for additional details, see Materials and Methods).

currents was not attributable to changes in recording parameters, because series resistance (R_s) and leak currents (I_L) (at $V_h = -75$ mV) did not change significantly (control, $R_s = 10.4 \pm 1.5$ MΩ, $I_L = -204 \pm 46$ pA; DHPG for 2 min, $R_s = 10.4 \pm 1.8$ MΩ, $I_L = -233 \pm 49$ pA, $n = 9$; $p > 0.05$). When probed at near physiological temperatures (30.8 ± 0.3°C, $n = 8$), T-type potentiation by 20 μM DHPG was increased to 87% ± 17% ($n = 8$, $p < 0.02$) (supplemental Fig. 1, available at www.jneurosci.org as supplemental material).

Bath application of DHPG is relatively slow and may lead to receptor desensitization. To better probe the time course of the T-type current modulation, we puffed DHPG locally above the PC dendritic tree (Tempia et al., 2001) (see Materials and Methods). Puff application of 100 μM DHPG caused a fast potentiation of T-type currents (45 ± 12%, $n = 6$) that reached a maximal level within 10 s (Fig. 2*D*). An increase in leak current likely attributable to the activation of sEPSCs was observed for the first two pulses after the DHPG puff ($I_L = -279 \pm 132$ pA, $n = 6$), but thereafter leak values returned to control levels ($I_L = -171 \pm 94$ pA, $n = 6$), whereas the T-type current potentiation remained. The puff-induced potentiation of T-type currents reversed by 94 ± 9% ($n = 6$) during perfusion of control solution (supplemental Fig. 2, available at www.jneurosci.org as supplemental material). Coapplication of DHPG with a group 1 antagonist (500 μM MCPG) or a specific mGluR1 antagonist (100 μM LY367385) abolished the T-type potentiation (−1.7 ± 3.3%, $n = 6$ and 0.5 ± 3.0%, $n = 8$, respectively), indicating that the potentiating effect of DHPG is mediated by mGluR1 subtype receptors (Figs. 2*C*, 3*B*).

The heterologous expression analyses in transfected HEK 293 cells indicated that both $Ca_v3.1$ and $Ca_v3.2$ T-type channel isoforms were capable of being upregulated by mGluR1 activation (Fig. 1). Because PCs are reported to express the $Ca_v3.1$ and $Ca_v3.3$ T-type Ca^{2+} isoforms but not $Ca_v3.2$ (Talley et al., 1999; Molineux et al., 2006), the observed T-type current upregulation in PCs was predicted to be attributable to native $Ca_v3.1$ channel modulation. To confirm the identity of the Ca_v3 isoform that underlies the potentiated T-type current in PCs, we recorded neurons from $Ca_v3.1$ T-type channel gene KO mice (P8–P12). Figure 2*E* shows that PCs from $Ca_v3.1$ KO mice completely lacked T-type whole-cell currents during depolarizing test pulses to −40 mV, whereas wild-type (WT) mice exhibited robust currents under these conditions ($Ca_v3.1$ KO, 12 ± 16 pA, $n = 4$; WT, 1280 ± 85 pA at −40 mV, $n = 3$). As observed in rat PCs, the T-type currents of WT mice are significantly potentiated by DHPG application (Fig. 2*F*). We conclude that the modulated T-type currents of immature rodent PCs are principally mediated by $Ca_v3.1$ channels.

R-type Ca^{2+} channels are reported to be expressed in PCs (Meacham et al., 2003) and share some voltage-dependent and kinetic properties with T-type channels (Soong et al., 1993; Li et al., 2007). The fact that 50 μM Ni^{2+} was included in our external solution to block $Ca_v2.3$ (R-type) currents argues against a potential contamination by $Ca_v2.3$ channels (Zamponi et al., 1996).

However, to fully rule out this possibility, we examined PCs in $Ca_v2.3$ gene KO mice (P8–P12). Figure 2*F* shows that the DHPG-induced Ca^{2+} current potentiation in PCs was similar in both $Ca_v2.3$ KO and WT mice. Together, our findings demonstrate that mGluR1 activation in PCs specifically and selectively potentiates T-type currents that are mediated by $Ca_v3.1$ T-type channels.

mGluR1 potentiates T-type currents through an increase in maximal current and a shift in the voltage dependence of activation

To characterize the underlying biophysical basis of the mGluR1-mediated potentiation, the voltage dependence of the rat (P8–P12) PC T-type currents was quantified using a series of test depolarizations ranging from −70 to −5 mV. To minimize the effects of contaminating HVA Ca^{2+} currents (especially P-type) and K^+ currents in this broader voltage range, higher concentration antagonists were used that included 300 μM Cd^{2+}, 10–20 mM TEA^+, and 5–10 mM 4-AP. Peak T-type currents increased significantly ($p < 0.05$) in response to bath application of 30 μM DHPG at all potentials between −45 and −20 mV (Fig. 2*G*). DHPG application also caused a significant (−2.4 mV, $n = 7, p < 0.02$) shift in the half-activation potential (V_{50act}) of the T-type currents but had no significant ($p > 0.05$) effect on the voltage dependence of T-type steady-state inactivation (Fig. 2*H*) (supplemental Table 1, available at www.jneurosci.org as supplemental material). These results indicate that the DHPG-induced potentiation is mediated by both an increase in maximal current, suggesting a change in open probability and/or conductance of the channels, and a shift in the voltage dependence of activation.

mGluR1 potentiates T-type currents through a G-protein-, tyrosine phosphatase/kinase-, and $[Ca^{2+}]$-dependent pathway

Multiple intracellular signaling pathways are known to be associated with mGluR1s in PCs (Knöpfel and Grandes, 2002), and we set out to study the identity of the signaling components leading to T-type current potentiation. Inclusion of 2 mM GDP-β-S in the pipette solution to block G-protein activity (Gα and Gβγ) completely abolished the potentiation of rat (P8–P12) PC T-type currents by DHPG (Fig. 3*A*, *B*). However, blocking phospholipase C (PLC) with either 1 μM U73122 (Fahlman et al., 2002) or 10 μM edelfosine

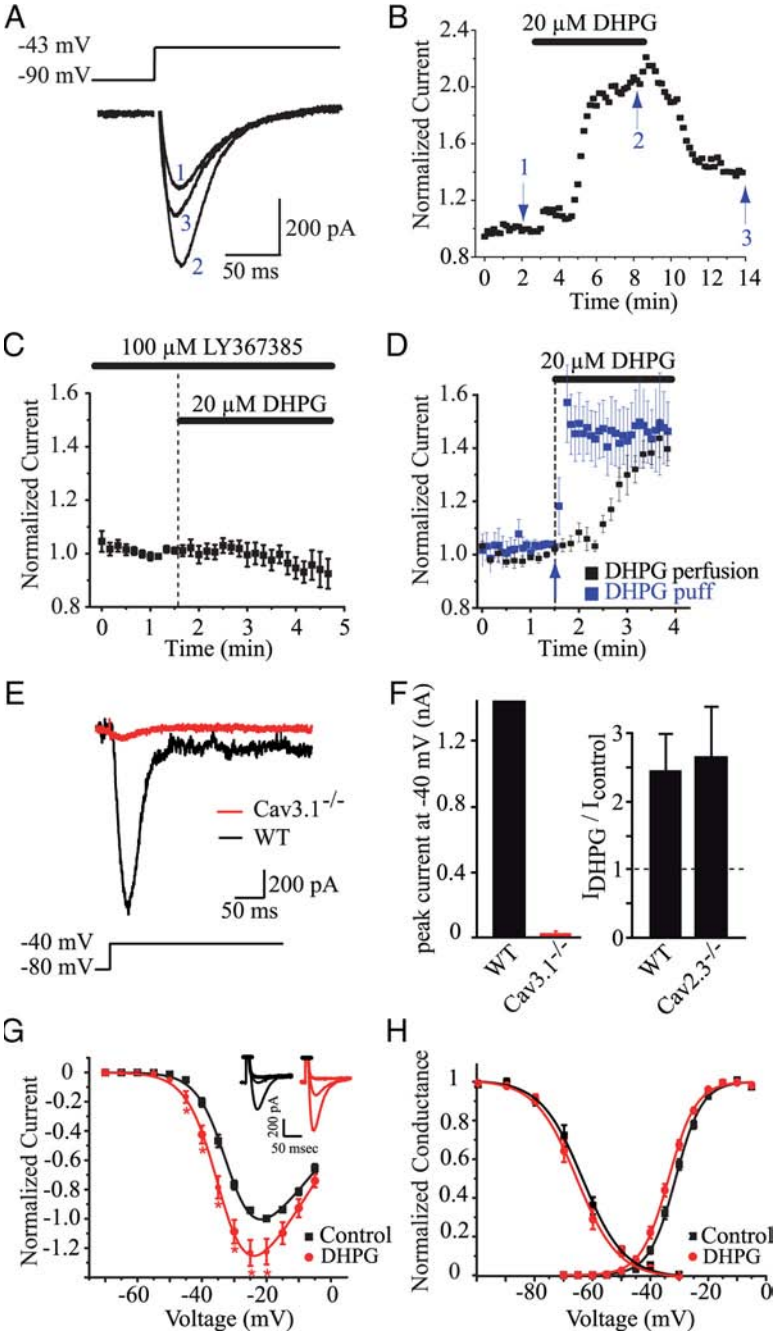

Figure 2. T-type Ca^{2+} currents are potentiated by mGluR1 activation in young cerebellar Purkinje neurons. ***A***, Representative voltage-clamped current traces for rat PC T-type currents during depolarizing pulses from −90 to −43 mV before (1), during (2), and after (3) activation of endogenous mGluR1s with 20 μM DHPG. ***B***, Normalized peak current time course for the same cell in ***A*** demonstrating the reversibility of DHPG-induced potentiation. ***C***, DHPG stimulates T-type currents specifically through mGluR1s. Blocking mGluR1 with perfusion of 100 μM LY367385 ($n = 8$) for 20 min before and during DHPG application abolished potentiation. ***D***, Average normalized peak T-type current time course during control perfusion followed by either bath perfusion of 20 μM DHPG (black plot; T-type currents increased by 51 ± 7%, $n = 19$ after 100–120 s of DHPG application) or a picospritzer puff (50 ms, 10 psi) of DHPG (100 μM) that shows a rapid potentiation of T-type current amplitude by 45 ± 12% ($n = 6$; blue plot). ***E***, Representative current traces during depolarizations from −80 to −40 mV in WT (black) and $Ca_v3.1^{-/-}$ (red) mice. ***F***, Left, Quantification of peak PC T-type currents in $Ca_v3.1^{-/-}$ mice ($n = 4$) compared with WT mice ($n = 4$) during depolarizing steps to −40 mV. Right, DHPG (20 μM) causes robust and equal T-type potentiation in WT mice ($n = 3$) and $Ca_v2.3^{-/-}$ mice ($n = 4$). ***G***, Normalized *I–V* curve showing that DHPG (red plot) increases maximal current, resulting in a significant potentiation of T-type currents at potentials between −45 and −20 mV ($n = 7$). *$p < 0.05$ compared with control current values. Inset, Representative voltage-clamped current traces from rat PCs during depolarizations to potentials ranging from −60 to −30 mV before (left) and after (right) mGluR1 was activated with 30 μM DHPG. ***H***, Normalized conductance curves for activation and steady-state inactivation fitted with Boltzmann equations (see Materials and Methods). DHPG application caused a small but significant ($p < 0.02$) shift of ~2 mV in the V_{50act} and had no significant ($p > 0.05$) effect on the steady-state inactivation ($V_{50inact}$) of T-type currents within PCs (supplemental Table 1, available at www.jneurosci.org as supplemental material).

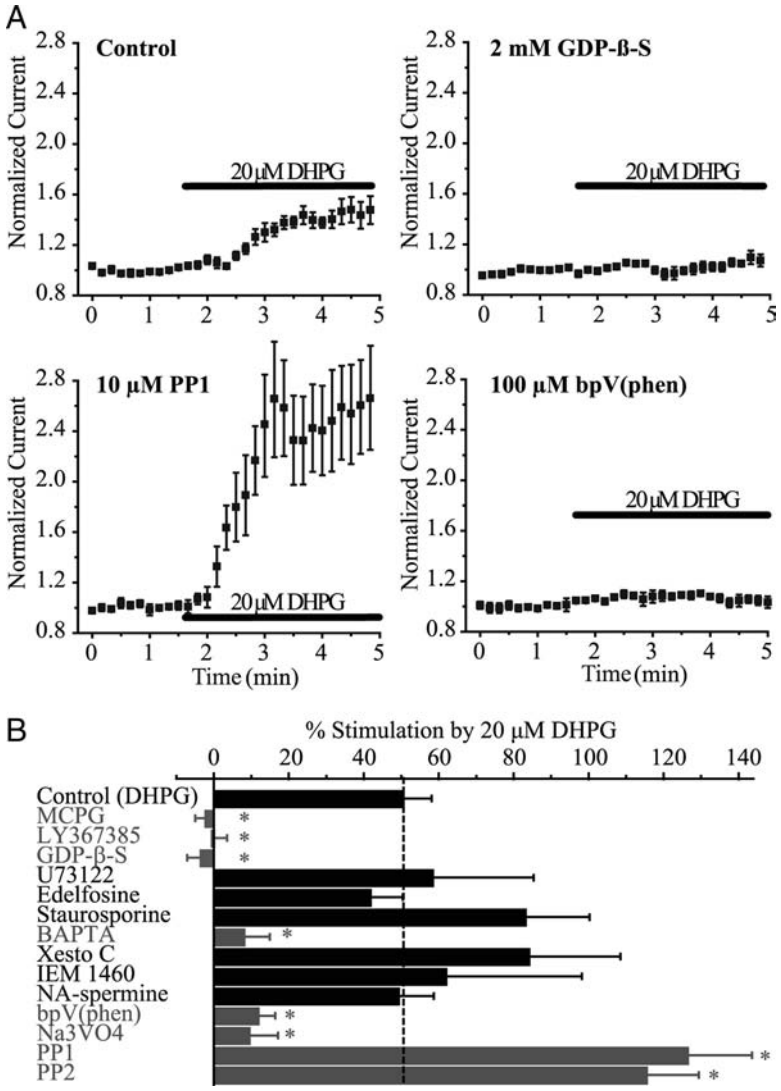

Figure 3. T-type Ca^{2+} currents are potentiated by mGluR1 through a signaling pathway that involves G-proteins, intracellular Ca^{2+}, and tyrosine phosphatases. ***A***, Top left, Control normalized time course showing the effects of DHPG application on voltage-clamped rat PC T-type currents in the absence of any other signaling antagonists (during depolarizations from −90 mV to between −50 and −40 mV). Top right, Potentiation of T-type currents via mGluR1 requires G-protein activation. Substitution of 2 mM GDP-β-S ($n = 5$) for GTP in the intracellular pipette solution for 10 min in the whole-cell conformation eliminated DHPG-induced potentiation. Bottom left, Potentiation of T-type currents by DHPG is enhanced by blocking tyrosine kinase activity. Blocking Src-family tyrosine kinases with inclusion of 10 μM PP1 in the pipette ($n = 5$) augmented the DHPG-induced increase. Bottom right, Potentiation of T-type currents by DHPG requires tyrosine phosphatase activity. Blocking tyrosine phosphatases via perfusion of 100 μM bpV(phen) ($n = 6$) for 10 min before and during DHPG application attenuated the potentiation effect. ***B***, Histogram showing potentiation values compared with the control (DHPG) potentiation value for the above results as well as for other antagonists. Blocking group I mGluRs with 500 μM MCPG ($n = 6$), buffering intracellular Ca^{2+} through inclusion of 20 mM BAPTA ($n = 6$) in the pipette, and blocking tyrosine phosphatases with 1 mM Na_3VO_4 ($n = 5$) all significantly (gray bars; $p < 0.02$) reduced the DHPG-induced increase. Blocking Src-family tyrosine kinases with inclusion of 10 μM PP2 in the pipette ($n = 6$) significantly ($p < 0.02$) augmented the DHPG-induced increase. Blocking phospholipase C with 1 μM U73122 ($n = 6$) or 10 μM edelfosine ($n = 7$), serine/threonine kinases (such as protein kinase C) with 1–2.5 μM staurosporine ($n = 8$), IP_3Rs with 1 μM xestospongin C ($n = 6$), and sEPSC currents with 250 μM IEM 1460 ($n = 6$) or 100 μM NA-spermine ($n = 5$) all caused no significant ($p > 0.05$) change in the level of DHPG-mediated increase in T-type currents. All potentiation values were calculated 100–120 s after initiation of DHPG application, except for NA-spermine and edelfosine, in which the effect was calculated 60–80 s into potentiation (equivalent time from start of potentiation to other groups), because the effect was delayed. *$p < 0.02$.

(Horowitz et al., 2005), PKC with 1 to 2.5 μM staurosporine (Shin et al., 2007), or IP_3 receptors (IP_3Rs) with 1 μM xestospongin C (Izumi et al., 2000) all had no significant ($p > 0.05$) effect on the DHPG-mediated increase in T-type currents (Fig. 3*B*). As cited, all antagonists that had negative results have been shown previously to be effective at the given concentrations within brain slice recordings. Similar to our findings, Canepari and Ogden (2003) showed that activation of sEPSCs by mGluR1 was dependent on G-protein activation but independent of PLC activation. In these experiments, the authors found that sEPSC activation depended on tyrosine phosphatase activity. Accordingly, in our experiments, blocking tyrosine phosphatase activity with either 1 mM Na_3VO_4 or its more potent analog 100 μM bpV(phen) caused a significant ($p < 0.02$) attenuation of T-type current potentiation by DHPG (Fig. 3*A*, *B*). Furthermore, Src-family tyrosine kinase inhibitors (10 μM PP1 or PP2 in recording pipette) significantly ($p < 0.02$) enhanced the potentiation effect (Fig. 3*A*,*B*). These findings strongly suggest that sites of tyrosine phosphorylation control mGluR1-mediated $Ca_v3.1$ T-type potentiation.

Interestingly, the potentiation of T-type currents by mGluR1 also depended on intracellular Ca^{2+} concentration $[Ca^{2+}]_i$, because buffering $[Ca^{2+}]_i$ with 20 mM intracellular BAPTA in the recording pipette significantly ($p < 0.02$) reduced the effect (Fig. 3*B*). To test whether the Ca^{2+}-permeable sEPSC was directly involved in the potentiation of T-type currents by mGluR1, antagonists of this current [250 μM IEM 1460 or 100 μM naphthylacetyl (NA)-spermine (Canepari et al., 2004)] were preapplied and coapplied with DHPG and found to have no significant effect on the potentiation magnitude (Fig. 3*B*). The antagonist often used to block TRPC currents (Kim et al., 2003), SKF 96365, was not used here because we observed it to potently block T-type currents (data not shown) (see Materials and Methods). Overall, it appears that mGluR1 activates a G-protein and tyrosine-phosphatase-dependent pathway upstream of PLC activation that positively modulates both sEPSC and $Ca_v3.1$ T-type currents independently of each other.

$Ca_v3.1$ channels are predominantly localized to dendritic spines in young and mature mice

T-type Ca^{2+} channels have been identified in both the dendrites and spines of PCs (Mouginot et al., 1997; Isope and Murphy, 2005), whereas mGluR1s and TRPC channels are enriched at the PF–PC and climbing fiber (CF)–PC synapses (Baude et al., 1993; Kim et al., 2003; Hartmann et al., 2008). To address the localization of the functional interaction between T-type channels and mGluR1s, we developed a subtype-specific polyclonal antibody against $Ca_v3.1$ channels (see Materials and Methods). The previous voltage-clamp electrophysiological experiments (Figs. 2, 3, 6) were performed on immature PCs (P8–P12), whereas subsequent presynaptic stimulation imaging experiments (see Figs. 7, 8) were performed

in mature PCs of older mice (P15–P25). In this regard, we performed immunohistochemistry assays both on juvenile (P15) and adult (P60) mice. We did not detect any staining differences between young and adult mice. Figures 4 and 5 present data from adult mice, and the immunohistochemical data from young animals is summarized in supplemental Figure 3 (available at www.jneurosci.org as supplemental material).

Figure 4*A* shows strong $Ca_v3.1$ immunoreactivity in the cerebellum and thalamus of WT control mice, with weaker staining observed in other brain regions. Confirming the specificity of the antibody, $Ca_v3.1$ immunoreactivity was reduced to background levels in $Ca_v3.1^{-/-}$ KO mice (Fig. 4*B*). Using the $Ca_v3.1$-selective antibody, we then determined the cellular expression and subcellular localization of $Ca_v3.1$ channels in the cerebellum by double immunofluorescence (Fig. 4*D–H*), preembedding immunoelectron microscopy (Fig. 5*A–F*), and postembedding immunogold microscopy (Fig. 5*G–I*).

In the cerebellum, the highest level of $Ca_v3.1$ immunoreactivity was found in the molecular layer (Fig. 4*C–H*). Weaker but clear expression was also observed in other neurons, including basket, Golgi, and unipolar brush cells (data not shown). In the molecular layer, punctuate $Ca_v3.1$ labeling overlapped that of calbindin staining (a marker for PCs) in tiny bulges around the spiny branchlets of PCs (Fig. 4*D*). Presynaptic $Ca_v3.1$ labeling was not discernible in the varicosities of PFs (vesicular glutamate transporter VGluT1 staining), CFs (VGluT2 staining), and inhibitory neurons (vesicular GABA transporter VGAT staining) (Fig. 4*E–G*). Rather, $Ca_v3.1$ puncta appeared to appose extensively to VGluT1-positive PF terminals (Fig. 4*E*) and also to VGluT2-positive CF terminals (Fig. 4*F*). Specific immunoreactivity for $Ca_v3.1$ was also observed inside the perikarya and shaft dendrites of PCs but was weaker and more diffuse compared with the neuropil puncta. Overall, these findings suggest that $Ca_v3.1$ channels are highly concentrated in the spines of PC dendrites. Double immunofluorescence with mGluR1 (Fig. 4*H*) showed an extensive overlapping with $Ca_v3.1$ staining in spines, whereas $Ca_v3.1$ puncta inside dendritic shafts (asterisks in Fig. 4*H*) poorly overlapped with mGluR1 labeling. This suggests an extensive colocalization of $Ca_v3.1$ T-type channels and mGluR1s in PC dendritic spines.

The localization of $Ca_v3.1$ T-type channels within dendritic compartments was further refined using immunoelectron microscopy. Preembedding immunoperoxidase reactions stained the cytoplasm of PC spines (Fig. 5*A*,*C*) and dendrites (Fig. 5*B*). These immunolabeled PC elements formed synaptic contacts with PFs (Fig. 5*A*), CFs (Fig. 5*C*), and inhibitory terminals (data not shown). Using a silver-enhanced immunogold technique, most metal particles found in dendritic spines were associated with the cell membrane, whereas in dendritic shafts many particles were distributed intracellularly around vesicles or cisterns of the smooth endoplasmic reticulum (Fig. 5*D–F*). No significant labeling was detected in the postsynaptic density or in presynaptic terminals and axons, including the active zone. Because of dense molecular environments, antigens condensed at the synaptic junction are often protected from the penetration and binding of antibodies (Fritschy et al., 1998; Watanabe et al., 1998). This effect can be overcome by postembedding immunogold (Ottersen and Landsend, 1997). Using this approach, the postembedding method reproduced preferential $Ca_v3.1$ labeling of the extrasynaptic cell membrane in dendritic spines (Fig. 5*G*,*H*) and of intracellular sites in dendritic shafts (Fig. 5*I*). No significant labeling was observed in the synaptic junctional membranes. Together, we concluded that, in mature (Figs. 4, 5) and immature (supplemental Fig. 3, available at www.jneurosci.org as supplemental material) mice, $Ca_v3.1$ channels are expressed on the extrasynaptic surface of PC spines that form excitatory synapses with PFs and CFs and are in close proximity to mGluR1s.

mGluR1 potentiates T-type Ca^{2+} transients at synaptic sites

Given the anatomical and functional coupling between mGluR1s and $Ca_v3.1$ T-type Ca^{2+} channels, we then assessed whether a direct modulation of T-type Ca^{2+} influx could be detected within specific PC cellular compartments. We monitored Ca^{2+} transients quasi-simultaneously in multiple spines and dendrites from PCs of P8–P12 rats using random access multiphoton microscopy (Fig. 6). In the example shown, 40 POIs were imaged at a frame rate near 1 kHz. Whole-cell voltage-clamp experiments were performed in the same conditions as Figures 2 and 3 except that heparin (4 mg/ml) was included in the patch pipette to block the contaminating effect of Ca^{2+} increases through the mGluR1-activated IP_3R pathway. T-type channel-mediated Ca^{2+} transients were observed throughout the PC dendritic tree and the soma (Fig. 6*B*), as shown previously (Isope and Murphy, 2005). Notably, DHPG application (20 μM) increased the Ca^{2+} transients ($\Delta F/R$; see Materials and Methods) in spines and proximal dendrites but not in parent dendrites (Fig. 6*B*) or at the soma (data not shown). The time course of this potentiation was correlated to the increase of T-type currents recorded at the soma, as exemplified for the averaged spine Ca^{2+} transient in Figure 6, *C* and *D*.

To quantitatively assess the localization of the DHPG effect, PCs were divided into four compartments: soma, proximal dendrites, distal dendrites, and spines. All the POIs for all the cells recorded were then pooled by compartment, normalized by the density of current in each cell, and averaged together (Fig. 6*E*). Histograms in Figure 6*E* show that the Ca^{2+} transients, which are largest in spines, are significantly potentiated by DHPG in both spines ($p < 0.001$, Wilcoxon's rank test) and proximal dendrites ($p < 0.01$, Wilcoxon's rank test) but not in the shaft of spiny branchlets (distal dendrites) or at the soma. In another set of imaging experiments, heparin was omitted from the pipette solution. When the IP_3-mediated release from internal Ca^{2+} stores was intact, DHPG also increased the Ca^{2+} transients in the shaft of the spiny branchlets (Fig. 6*E*). These findings suggest that the potentiation of T-type channels is restricted to the vicinity of mGluR1s, at PF and CF contacts in the spines and proximal dendrites, respectively, as suggested by the immunohistochemistry staining (Fig. 4), whereas Ca^{2+} released from internal stores can relay the effect of mGluR1 activation to the dendritic shafts. Although the current paper focuses on the physiological implications of T-type potentiation at PF–PC synapses within PC spines, the potentiation of T-type currents at CF–PC synapses in the proximal dendrites could have significant effects on PC excitability, such as generating mGluR1-mediated dendritic Ca^{2+} transients and altering firing thresholds (Yuan et al., 2007). These possibilities are currently under investigation.

Burst stimulations of parallel fibers trigger T-type Ca^{2+} influx in mature PCs of older mice

$Ca_v3.1$ T-type channels appear ideally located in the spine head to participate in Ca^{2+} signaling during PF activity. In this regard, we assessed the physiological role of $Ca_v3.1$ channels during trains of PF stimulation (2–13 stimulations at 100 Hz every 30 s), a physiological mode of granule cell discharge (Chadderton et al., 2004; Jörntell and Ekerot, 2006) that is known to evoke depolarization-induced Ca^{2+} transients within spines (Denk et

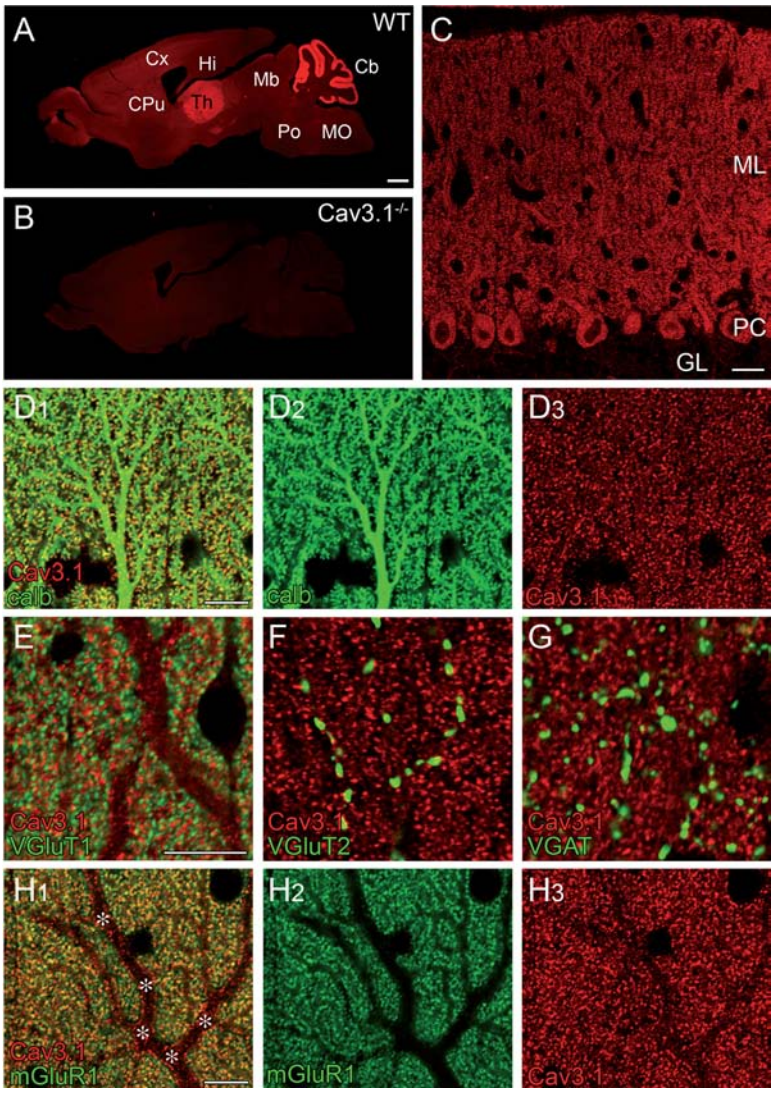

Figure 4. Immunofluorescence showing predominant distribution of $Ca_v3.1$ in the dendritic spines of cerebellar Purkinje cells. ***A***, ***B***, Specificity of $Ca_v3.1$ immunohistochemistry in the mouse brain. Note intense immunofluorescence labeling in the cerebellum (Cb) and thalamus (Th) of WT (***A***) but not $Ca_v3.1^{-/-}$ mice (***B***). CPu, Caudate–putamen; Cx, cortex; Hi, hippocampus; Mb, midbrain; MO, medulla oblongata; Po, pons. Scale bar, 1 mm. ***C***, Single immunofluorescence for $Ca_v3.1$ in the cerebellar cortex. GL, Granular layer; ML, molecular layer. Scale bar, 20 μm. ***D–H***, Double immunofluorescence for $Ca_v3.1$ (red) and other molecules (green) in the cerebellar molecular layer. Asterisks in H_1 indicate shaft dendrites of PCs. Note punctate $Ca_v3.1$ labeling in the neuropil, which overlaps extensively with calbindin (calb; ***D***) and mGluR1 (***H***) in putative dendritic spines but not with VGluT1 (***E***), VGluT2 (***F***), or VGAT (***G***) in excitatory and inhibitory presynaptic terminals. Scale bars, 10 μm.

al., 1995; Finch and Augustine, 1998; Takechi et al., 1998). Experiments were performed in WT or $Ca_v3.1$ KO mice (P15–P25 mice) in the current-clamp mode using a K^+-based internal solution and a near physiological temperature (32–34°C). Heparin was included in the patch pipette, and cyclopiazonic acid (6 μM) was added to the bath perfusion (except in Fig. 7*B*) to ensure a complete block of store-mediated Ca^{2+} signaling (Finch and Augustine, 1998; Takechi et al., 1998). In all experiments, AM 251 [*N*-(piperidin-1-yl)-5-(4-iodophenyl)-1-(2,4-dichlorophenyl)-4-methyl-1*H*-pyrazole-3-carboxamide] a cannabinoid receptor antagonist, and bicuculline were also perfused to prevent presynaptic depression of the PF input (Maejima et al., 2005; Crepel and Daniel, 2007).

In WT animals, all cells tested displayed a small and graded local Ca^{2+} transient in PC spiny branchlets (mean signal $\Delta F/R$ = 4.7 ± 1.2%, n = 6, for 13 pulses at 100 Hz and V_h = −75 mV) (Fig. 7*A*). Moderate stimulation strength was used, as assessed from the amplitude of the first somatic EPSP in the train (mean unitary EPSP size, 3.3 ± 2.0 mV, n = 12) (Fig. 7). At these low stimulation intensities, the Ca^{2+} influx was localized to a small number of spiny branchlets and decreased to an undetectable level in the surrounding dendrites (Fig. 7*A*). Calcium influx was fast, peaking within tens of milliseconds after the stimulation, which decreases the possibility that the Ca^{2+} transients were attributable to the much slower (~200 ms) opening of TRPC channels (Kim et al., 2003; Hartmann et al., 2008). Additionally, the Ca^{2+} transients were never recorded for a single stimulation (n = 7); rather, they appeared after two to three stimulations and increased for each of the following stimulations (n = 7) (Fig. 7*B*, *C*). Thus, activation of Ca^{2+} transients at PF–PC synapses requires a summated burst of activity.

The spontaneous pacemaker activity of PCs may affect dendritic transients evoked by PF stimulations. However, somatic Na^+ spikes eventually evoked by PF stimulations were not associated with an increased amplitude or spatial extent of the dendritic Ca^{2+} transient. Nonetheless, we performed a series of experiments in which cells (n = 7) were alternatively held at V_h = −70 mV or left to spike at their own pace (from 20 to 50 Hz) by removing the hyperpolarizing current injection. The Ca^{2+} transients did not increase significantly with depolarization (control, $\Delta F/R$ = 3.7 ± 0.4%; depolarized, $\Delta F/R$ = 4.1 ± 0.4%; n = 5) (Fig. 7*B*), suggesting that membrane potentials in distal parts of the dendritic tree are only slightly affected by membrane potential changes at the soma. In two other cells, depolarization combined with trains of at least four stimulations elicited a small plateau potential or an upstate in the PC that was correlated with a huge increase in the $\Delta F/R$ signal (10.4-fold in one cell, 4.4-fold in the other cell), suggesting the activation of HVA Ca^{2+} channels (supplemental Fig. 4, available at www.jneurosci.org as supplemental material), as shown previously by dendritic patch recordings (Rancz and Hausser, 2006). In some spines (supplemental Fig. 5, available at www.jneurosci.org as supplemental material), a slow delayed Ca^{2+} transient, which might be attributed to TRPC channel opening, summed on the large and fast Ca^{2+} influx. Calcium spikes could also be induced at hyperpolarized potentials but with a high threshold of ~5 mV for the first EPSP (data not shown).

Finally, the mean $\Delta F/R$ was reduced to 1.2 ± 0.3% (n = 6; mean unitary EPSP size, 3.46 ± 2.27 mV, n = 5) in $Ca_v3.1^{-/-}$ mice (Fig. 7*D*, white bars), demonstrating that the vast majority of the local Ca^{2+} transient is mediated by $Ca_v3.1$ T-type Ca^{2+}

channels. Thus, under our conditions, T-type Ca^{2+} signaling precedes local HVA Ca^{2+} spikes, which are associated with synchronous activation of many PFs within a local beam.

mGluR1s modulate T-type Ca^{2+} transients at individual spines during parallel fiber high-frequency bursts

Burst stimulations of PF beams are known to activate mGluR1s (Batchelor and Garthwaite, 1997), and potentiation of $Ca_v3.1$ T-type channels by mGluR1 might act to amplify the PF-evoked Ca^{2+} influx. In WT mice (P15–P25), perfusion of JNJ16259685 (1.5 μM), a potent and specific antagonist of the mGluR1 (Knöpfel, 2007), strongly reduced local Ca^{2+} transients within 2 min of its application (control, $\Delta F/R = 4.7 \pm 1.2\%$; JNJ, $\Delta F/R = 2.5 \pm 0.9\%$; $n = 6$) (Fig. 7*D*,*E*). No effect was observed after application of JNJ in $Ca_v3.1$ KO mice (control, $\Delta F/R = 1.2 \pm 0.3\%$; JNJ, $\Delta F/R = 1.0 \pm 0.3\%$; $n = 6$) (Fig. 7*D*). The variation in the magnitude of the potentiation during trains of different length suggests that the mGluR1-mediated potentiation of the local Ca^{2+} transients occurs as early as the third pulse in the train, i.e., 10–30 ms (Fig. 7*C*). Thus, $Ca_v3.1$-mediated Ca^{2+} transients evoked by bursts of PF EPSPs are strongly potentiated by synaptic mGluR1 activation. This feature was observed with no significant difference between any of the ages tested (P15–P25) (supplemental Fig. 6, available at www.jneurosci.org as supplemental material).

Parallel fiber-induced EPSPs spread electrotonically into the dendritic arborization of the PC and may open T-type Ca^{2+} channels along the spiny branchlets and dendritic shafts. However, the preferential extrasynaptic expression and functional coupling between $Ca_v3.1$ and mGluR1 within PC spines may greatly favor T-type Ca^{2+} signaling within active spines. To test this hypothesis, we performed a quasi-simultaneous quantitative mapping of Ca^{2+} transients at multiple POIs located in the vicinity of the stimulated PF beam. Figure 8*A* shows that, in a given spiny branchlet, JNJ16259685 perfusion blocks the PF-induced Ca^{2+} transients in some spines (spines 1 and 4) but does not affect others (spines 2 and 3). When the $\Delta F/R$ signal in JNJ was plotted against the $\Delta F/R$ signal in the control condition for this cell, we observed a population of POIs with a strong mGluR1 effect (points below bisector line) and a remaining population with no apparent mGluR1 potentiation (points on/near bisector line). A statistical *t* test was applied to all the individual POIs to compare the mean $\Delta F/R$ in the control condition versus the mean $\Delta F/R$ during JNJ application for all recorded neurons in both WT mice ($n = 224$, $n = 5$ cells) and $Ca_v3.1^{-/-}$ mice ($n = 274$, $n = 5$ cells) (Fig. 8*B*). Points of interest displaying a significant attenuation by JNJ are plotted in green (Fig. 8*B*). In WT mice, we observed a population of POIs on the bisector line (in black) and another population located significantly below the bisector line (in green), indicating that JNJ treatment decreased the T-type Ca^{2+} transients (control, $\Delta F/R =$

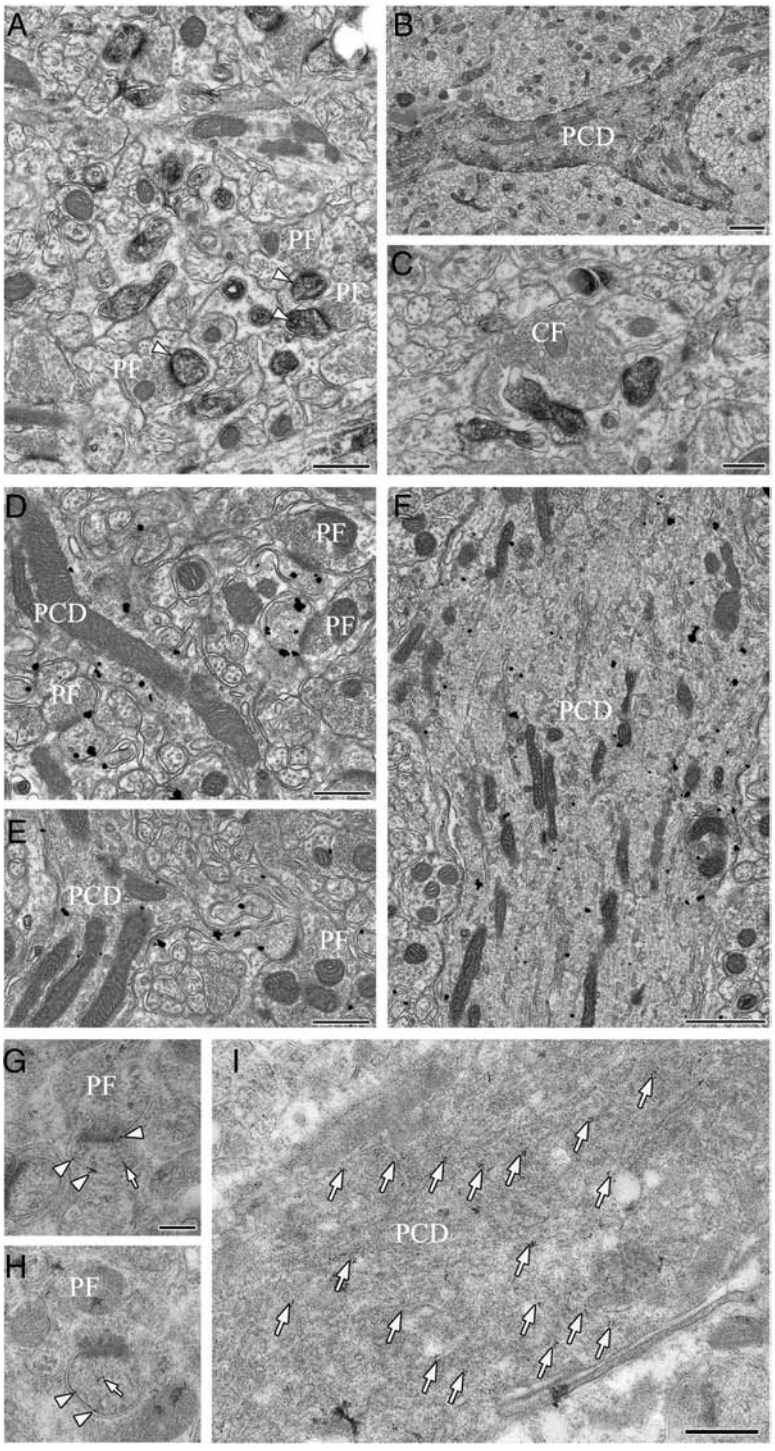

Figure 5. Immunoelectron microscopy showing predominant localization of $Ca_v3.1$ on the extrasynaptic surface of dendritic spines in cerebellar Purkinje cells. ***A–C***, Immunoperoxidase. Note intense labeling of $Ca_v3.1$ (arrowheads) in dendritic spines and shafts of PCs. ***D–F***, Preembedding silver-enhanced immunogold showing predominant surface labeling in dendritic spines, in contrast to intracellular labeling in dendritic shafts. ***G–I***, Postembedding immunogold. Arrowheads and arrows indicate gold particles associated with the cell membrane or distributed intracellularly, respectively. PCD, Purkinje cell dendrite. Scale bars: ***A***, ***C–E***, 500 nm; ***B***, ***F***, ***I***, 1 μm; ***G***, 200 nm.

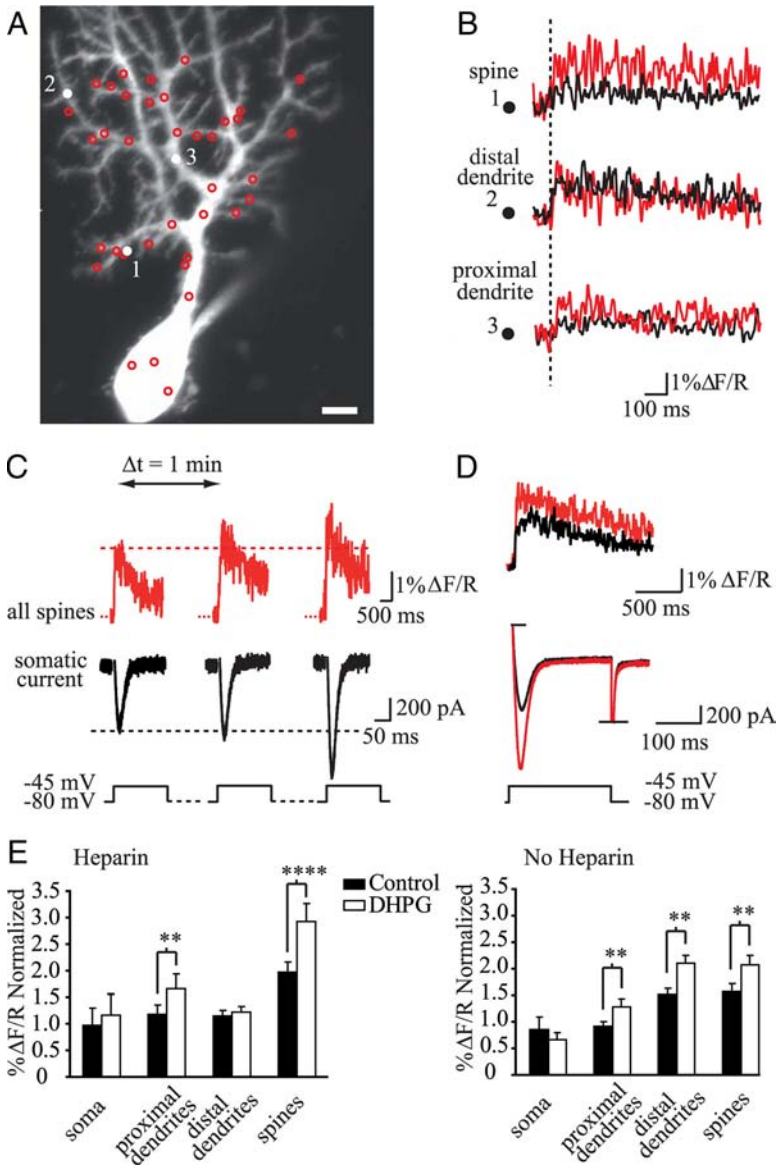

Figure 6. DHPG mediates an increase in T-type Ca^{2+} transients in Purkinje cells. ***A***, Two-photon image of a patch-clamped rat cerebellar PC. The dendritic regions outlined by circles are sites of imaging. Scale bar, 10 μm. ***B***, DHPG causes an increase in voltage-clamped low-threshold Ca^{2+} transients in spines and proximal dendrites when IP_3Rs are blocked. The Ca^{2+} transients ($\Delta F/R$; see Materials and Methods) at individual POIs during depolarizing steps from −80 to −45 mV at the soma are shown before (black) and after (red) application of 20 μM DHPG. Numbers refer to labels from ***A***. Traces were smoothed. The dotted vertical line indicates onset of the depolarizing pulse. Recordings were performed in the presence of 4 mg/ml heparin to block IP_3Rs. ***C***, The increase in low-threshold Ca^{2+} transients by mGluR1 activation coincides with the potentiation of T-type somatic currents. Three successive depolarizing pulses at the onset of the DHPG effect, starting 2 min after the beginning of the application, with 1 min between pulses. Average Ca^{2+} transients in all the POIs in the PC are shown in red. The red dotted line represents the standardized baseline Ca^{2+} level before the pulse; the red dashed line identifies the peak of fluorescence before the DHPG effect. In black, current recorded at the soma. The black dashed line identifies the peak current before the DHPG effect. ***D***, Top, The average Ca^{2+} transient in all imaged spines at all time points (10 s between sweeps) during the control period is shown in black (10 min total duration), and the average Ca^{2+} transient after onset of the DHPG effect is shown in red (5 min total duration). Middle, Mean current in control period (black) and during DHPG application (red). Bottom, Holding potentials. All data shown above in this figure are from the same cell. ***E***, Left, DHPG causes a potentiation of voltage-clamped T-type Ca^{2+} transients in the spines and proximal dendrites of PCs when IP_3Rs are blocked with heparin inclusion (4 mg/ml) in the patch pipette. Proximal dendrites, $n = 33$, 5 cells; distal dendrites, $n = 5$, 5 cells; spines, $n = 84$, 5 cells; soma, $n = 9$, 5 cells. Right, DHPG causes a potentiation of T-type Ca^{2+} transients in the spines, distal dendrites, and proximal dendrites of PCs when IP_3Rs are not blocked. Proximal dendrites, $n = 20$, 5 cells; distal dendrites, $n = 40$, 5 cells; spines, $n = 55$, 5 cells; soma, $n = 6$, 5 cells. $^{**}p < 0.01$, $^{****}p < 0.001$ (Wilcoxon's rank test). The values for $\%\Delta F/R$ Normalized are derived from the variation of the peak Ca^{2+} transient ($\Delta F/R$) normalized to the density of current at the soma (under control conditions; see Materials and Methods) in different compartments of the cell during the control period (black bars) and DHPG application (white bars).

4.2 ± 0.3%; JNJ, $\Delta F/R = 2.3 \pm 0.2\%$) in this second population of POIs (Fig. 8*B*). Moreover, 18 of 19 POIs with a $\Delta F/R$ above 9% in control conditions displayed a strong block by JNJ, suggesting that they were boosted by mGluR1 activation during PF bursts. Thus, the largest PF Ca^{2+} transients found in spines are mediated by mGluR1-potentiated $Ca_v3.1$ T-type channels. In comparison, in the $Ca_v3.1$ KO animals, the distribution of POIs was not biased, and the number of POIs with significant deviation (in green) were predicted by the stringency of the statistical test (5%) and were distributed on either side of the bisector line (control, $\Delta F/R = 0.53 \pm 0.02\%$; JNJ, $\Delta F/R = 0.47 \pm 0.06\%$) (Fig. 8*B*).

The presence, in WT mice, of POIs close to the bisector line (no difference in Ca^{2+} input between control and JNJ application) but with large transients argues in favor of a population of sites at which depolarization is the main determinant of T-type channel activity. However, focal electrical stimulations lead to a large number of spines simultaneously active in a given spiny branchlet. The larger summated depolarization might activate $Ca_v3.1$ channels strongly, reducing the role of the mGluR1 effect (Fig. 1*E*,*F*) and also eliciting Ca^{2+} input in spines that did not receive a synaptic input. For these reasons, we studied apparently nonresponding spiny branchlets surrounding the stimulation focus (Fig. 8*C*). In a few cases ($n = 3$), we found Ca^{2+} transients in responsive single spines that could be blocked by JNJ (Fig. 8*C*). These findings indicate that mGluR1 potentiation of T-type Ca^{2+} channels favors spine-specific Ca^{2+} signaling in PCs during physiological bursting activity of sparse PF inputs.

Discussion

$Ca_v3.1$ T-type Ca^{2+} channels expressed in Purkinje cells are potentiated by mGluR1

We find that T-type Ca^{2+} currents recorded in PCs from young rodents (P8–P12) are mainly mediated by $Ca_v3.1$ channels. It was reported previously that PC T-type currents from young animals have a low sensitivity to Ni^{2+}, indicating little functional expression of $Ca_v3.2$ channels, and that their biophysical properties matched closer with $Ca_v3.1$ rather than $Ca_v3.3$ currents (Isope and Murphy, 2005). Supporting these previous findings, we show here that T-type Ca^{2+} currents are undetectable in PCs from young $Ca_v3.1$ KO mice. Our results are also in agreement with *in situ* hybridization on

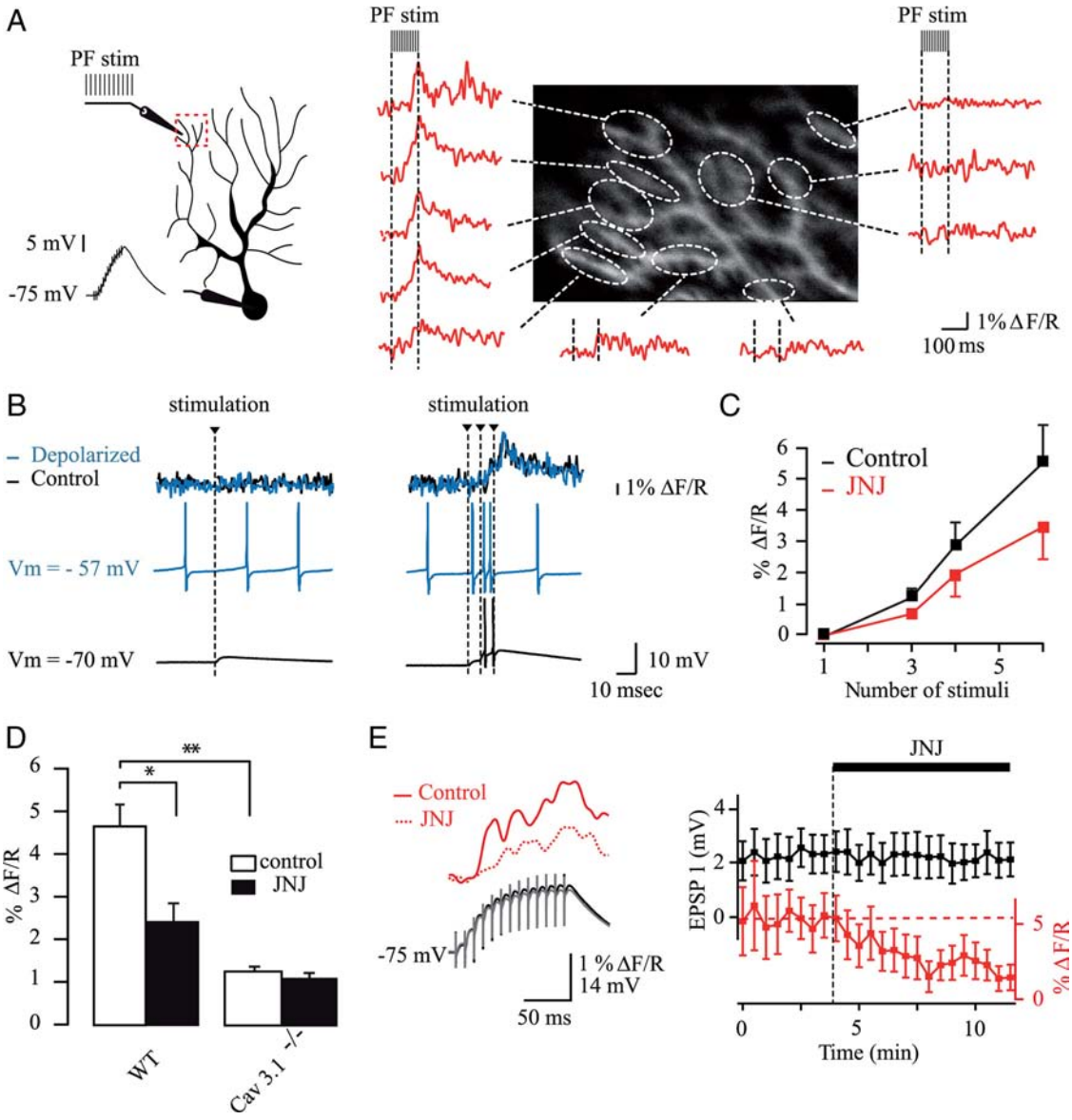

Figure 7. Parallel fiber stimulation activates mGluR1-potentiated T-type Ca^{2+} transients. ***A***, Left, Schematic drawing of experimental arrangement in mature mice (P15–P25). Inset, Representative EPSP recorded at the soma after PF stimulation. Right, Fluorescence transients ($\Delta F/R$) in spiny branchlets evoked by PF stimulation positioned on a two-photon section. In red, average fluorescence of three to seven POIs in the region of interest outlined with white dashed lines. Note the local and graded Ca^{2+} transients. The two black dashed lines indicate the duration of the PF stimulations (13 stimulations/100 Hz). ***B***, Fluorescence transients ($\Delta F/R$) in spiny branchlets evoked by 1 pulse (left) and three pulses (right) of PF stimulation at $V_h = -70$ mV (black) or with no injected current (blue). Right, There was no significant difference in the mean $\Delta F/R$ between control conditions (black) and depolarized conditions (blue, no current injected) (control, $\Delta F/R = 3.7 \pm 0.4\%$; depolarized, $\Delta F/R = 4.1 \pm 0.4\%$, $n = 5$). ***C***, Mean $\Delta F/R$ in control conditions (black) or during JNJ16259685 application for one, three, four, or six pulses in the PF train ($n = 3$). ***D***, Effect of JNJ16259685 application on the change of Ca^{2+} fluorescence in WT ($n = 6$) and $Ca_v3.1^{-/-}$ mice ($n = 6$). *$p < 0.05$, Wilcoxon's matched-pairs signed-ranks test. **$p < 0.01$, Wilcoxon's test. ***E***, Left, The PF-induced Ca^{2+} transient is attenuated after perfusion of JNJ16259685 (1.5 μM) (red dashed line). Each trace is an average of five consecutive trials. Fluorescence traces are an averaging of all responsive spiny branchlets. Right, Time course of the size of the first EPSP in the train (black) and the change of Ca^{2+} fluorescence (red) after perfusion of JNJ16259685 (1.5 μM) in the same set of cells tested with 11 pulses at 100 Hz ($n = 6$).

Sprague Dawley rats that revealed high expression levels of $Ca_v3.1$ in PCs (Talley et al., 1999). In adult PCs, we found that dendritic spines stain heavily for $Ca_v3.1$ channels, suggesting a role for this channel at synaptic sites (Fig. 4). This density of $Ca_v3.1$ channel expression is among the highest in the whole brain.

At the ultrastructural level, $Ca_v3.1$ channels are principally located at perisynaptic and extrasynaptic sites in the vicinity of mGluR1 sites as confirmed by double immunostaining (Fig. 4*H*) (supplemental Fig. 3, available at www.jneurosci.org as supplemental material), suggesting that $Ca_v3.1$ channels and mGluR1s are colocalized in PCs of both young and mature mice. In support, we found that T-type currents are potentiated by mGluR1 activation in both young and mature PCs. This potentiation occurred mainly in spines, whereas the modulation of dendritic shaft transients by mGluR1 depended on internal store activity (Fig. 6). Furthermore, we report that, in recombinant expression systems, mGluR1 modulation is subtype specific (Fig. 1), potentiating $Ca_v3.1$ and $Ca_v3.2$ isoforms while inhibiting $Ca_v3.3$ T-type channels. The latter is consistent with the known inhibition of $Ca_v3.3$ channels by $G\alpha_{q/11}$-coupled mAChRs (Hildebrand et al., 2007).

Molineux et al. (2006) provided immunohistochemical evidence for the expression of $Ca_v3.3$ in PCs of P14–P21 Sprague Dawley rats. A comparison with our data suggests that $Ca_v3.3$

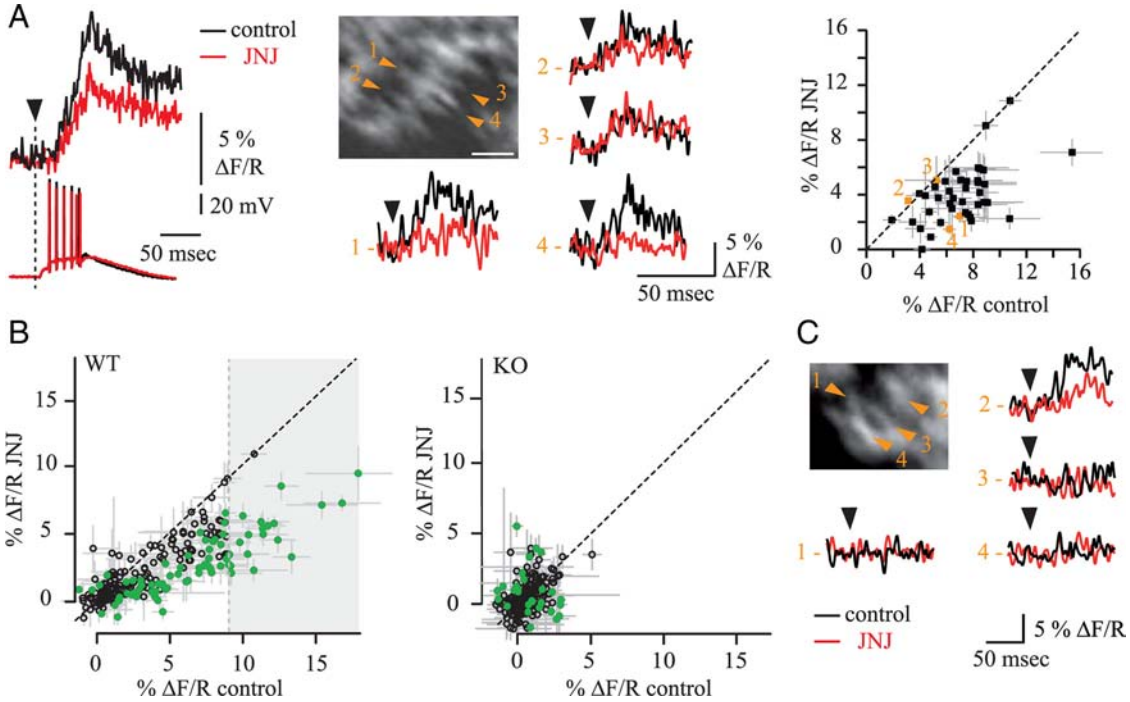

Figure 8. Spine-specific mGluR1 potentiation of T-type Ca^{2+} channels. ***A***, Left, Mean $\Delta F/R$ for all POIs in a cell in the control condition (black) or during JNJ application (red) correlated to mean EPSPs recorded at the soma. Middle, $\Delta F/R$ for individual spines in the control condition (black) or in JNJ (red) for the same cell. Orange labels refer to the POIs highlighted in the inset. Scale bar, 5 μm. Right, Plot of the $\Delta F/R$ for each POI in JNJ versus the control condition. Each $\Delta F/R$ is a mean of five consecutive trials at 0.05 Hz. The black dashed line represents the bisector line. ***B***, Plot of the $\Delta F/R$ for each POI in JNJ versus the control condition for of all the cells tested in WT (left; $n = 224$ POIs, 5 cells) and $Ca_v3.1$ KO (right; $n = 274$ POIs, 5 cells) mice. Each $\Delta F/R$ is a mean of five consecutive trials at 0.05 Hz. A green point illustrates a significant ($p < 0.05$) difference between control and JNJ application $\Delta F/R$ values. Black dashed line, Bisector line. Gray dashed line and rectangle highlight POIs for which control $\Delta F/R$ signal is above 9%. ***C***, Example of $\Delta F/R$ for labeled spines in the control condition (black) or in JNJ (red), demonstrating the activation and potentiation of a Ca^{2+} transient that is specific to an individual spine (label 2).

expression may increase during the third week of cerebellar development. Indeed, in our imaging experiments in 3- to 4-week-old $Ca_v3.1$ KO mice, a small component of the PF-induced Ca^{2+} transient remained and may be mediated by $Ca_v3.3$ (Fig. 7*D*). Interestingly, $Ca_v3.3$ staining was found exclusively in the dendritic shafts of the PC (Molineux et al., 2006) in which $Ca_v3.1$ localization is mostly cytoplasmic (Fig. 5*I*). $Ca_v3.3$-mediated low-threshold signaling in PC dendrites might amplify the contrast between spine and dendrite Ca^{2+} signals because mGluR1 activation inhibits $Ca_v3.3$ current as shown in HEK 293 cells (Fig. 1*C*).

The present study explored voltage-clamped T-type Ca^{2+} currents in young rats and mice (P8–P12), $Ca_v3.1$ and mGluR1 protein expression in both young (P15) and older mice (P60), voltage-clamped T-type Ca^{2+} transients in young rats (P8–P12), and physiologically stimulated T-type Ca^{2+} transients in older mice (P15–P25). The use of the various animal species and ages was necessary to address technique-specific experimental challenges ranging from adequate voltage clamping to developmental windows for PF–PC synaptogenesis. The combination of these multiple techniques demonstrated a robust functional interaction between mGluR1 and $Ca_v3.1$ that appears independent of species, age (between P8 and P25), or any specific recording method, and that can be observed at both room temperatures and more physiological temperatures.

Signal transduction pathway

As shown in Figure 1, activation of mGluR1a by glutamate in the HEK 293 expression system causes a potentiation of $Ca_v3.1$ and $Ca_v3.2$ currents with a slow and delayed onset. In contrast, mGluR1a activation causes a rapid and saturating inhibition of the $Ca_v3.3$ currents similar to that shown for the muscarinic modulation of $Ca_v3.3$ T-type currents in the same system (Hildebrand et al., 2007). Because the same $G\alpha_{q/11}$ protein is coupled to the metabotropic receptors that cause these modulations of $Ca_v3.1$, $Ca_v3.2$, and $Ca_v3.3$ currents, we postulate that different downstream transduction pathways in combination with specific channel isoforms determines the sign of the T-type modulation (Iftinca et al., 2007). Indeed, we have shown previously that the intracellular pathway leading to the inhibition of the $Ca_v3.3$ currents is independent from classical PLC/IP_3R pathways and is Ca^{2+} independent, but is partially $G\beta\gamma$ dependent. In contrast to this inhibition pathway, although the mGluR1-mediated potentiation of $Ca_v3.1$ currents within PCs is also PLC/IP_3R/Ca^{2+} store independent, it depends on tyrosine phosphatase activity and intracellular Ca^{2+} signals, because blocking tyrosine phosphatases or buffering intracellular Ca^{2+} attenuates the T-type current stimulation and blocking Src-family tyrosine kinases enhances the T-type potentiation. This PLC-independent, tyrosine-phosphatase-dependent pathway has been described previously at the PF–PC synapse by Canepari and Ogden (2003) between the mGluR1 and the sEPSC, identified as a nonspecific cationic channel TRPC (Kim et al., 2003; Hartmann et al., 2008) and also between mGluR1 and TRPC channels in hippocampal inhibitory interneurons (Topolnik et al., 2006). Canepari and Ogden showed that photolysis of glutamate in cerebellar slices activates the sEPSC via a G-protein and protein tyrosine kinase/phosphatase pathway. Similar to our results, a Src-family tyrosine kinase inhibitor enhanced the sEPSC, whereas tyrosine phosphatase inhibitors blocked this current. Inhibition of Src-family ty-

rosine kinases in PCs has also been shown recently to restore long-term depression that was abolished with mGluR1 blockade (Tsuruno et al., 2008). Because sEPSC antagonists (IEM 1460 or NA-spermine) have no effect on the T-type current modulation, the sEPSC channels and T-type channels appear to be independently regulated by mGluR1 activity. The known blockade of ionotropic glutamate receptors by these antagonists does not impact our conclusions, because AMPA/kainate receptors are already blocked by kynurenic acid in our signal transduction experiments.

Parallel fiber-induced fast Ca^{2+} influx is mediated by T-type Ca^{2+} channels and potentiated by mGluR1s in individual spines

We find that the local Ca^{2+} influx induced by trains of PF stimulations is reduced by >75% in $Ca_v3.1$ gene KO mice compared with WT mice. It should be noted that increasing the strength of the stimulations augments the density of active synapses on the spiny branchlet (as described by Wang et al., 2000), leading to additional depolarization that likely initiates opening of $Ca_v2.1$ P/Q-type channels (supplemental Fig. 4, available at www.jneurosci.org as supplemental material) and subsequent Ca^{2+} spike formation in a small number of spiny branchlets (as described by Rancz and Hausser, 2006).

Interestingly, we also find that a depolarized somatic membrane potential that enables spontaneous firing of the PC neither inactivates T-type channels nor promotes systematic activation of HVA Ca^{2+} channels, such as $Ca_v2.1$ channels, which are highly expressed in PCs. Our results then suggest that PC dendrites are actively clamped to hyperpolarized potentials. This notion is consistent with the previous observation that PC dendrites hyperpolarize when positive currents are injected at the soma (Rancz and Häusser, 2007). As described recently (Middleton et al., 2008), the activity of inhibitory oscillatory networks could also enhance the deinactivation of T-type channels in distal dendrites in some physiological conditions.

For moderate PF stimulations, the first EPSP in the train does not induce any Ca^{2+} influx, suggesting that mGluR1 activation and/or temporal summation are required to reach the threshold for T-type channel activation. Based on pairs of granule cell and PC recordings (Isope and Barbour, 2002), ~45 PF inputs (mean unitary connection, 8.4 pA; conversion factor, 8.3 μv/pA) are required to generate an EPSP of 3.2 mV at the soma (mean unitary value for the results in Fig. 7). Roth and Hausser (2001) showed that an EPSP recorded at the soma is attenuated by sixfold compared with synaptic locations, indicating that a 3.2 mV EPSP at the soma corresponds to a 19 mV depolarization at synaptic sites. Because hyperpolarized potentials are necessary to remove the inactivation of T-type currents, 19 mV might be too small to span the gap to the activation of T-type channels (Fig. 1). High-frequency bursts ~100 Hz may produce sufficient temporal summation to lead to T-type channel opening. In addition, recent results suggest the existence of a membrane potential overshoot in the spine head when compared with the parent shaft attributable to the neck resistance (Araya et al., 2006). This electrical amplification may be regulated, as assessed by measuring the spine–dendrite diffusion coefficient (Svoboda et al., 1996; Bloodgood and Sabatini, 2005), and could permit local T-type channel activation. By shifting the activation curve and potentiating T-type conductance at spines receiving a burst of EPSPs, mGluR1 activation could efficiently enhance the Ca^{2+} influx at the active spine relative to nearby inactive spines (Figs. 7, 8) that would lead to a specific tagging of the activated spine. This new voltage-dependant fast signaling pathway is triggered within 20 ms of the onset of the PF train and induces a strong boost of Ca^{2+} input within the spine compartment that might be essential for the local integration of the temporal code signal. Thus, the spine-specific potentiation of $Ca_v3.1$ channels by mGluR1 constitutes a major source of Ca^{2+} influx during physiological regimens of PF activity and may be involved in the induction of plasticity at PF synapses.

References

Aiba A, Kano M, Chen C, Stanton ME, Fox GD, Herrup K, Zwingman TA, Tonegawa S (1994) Deficient cerebellar long-term depression and impaired motor learning in mGluR1 mutant mice. Cell 79:377–388.

Anderson MP, Mochizuki T, Xie J, Fischler W, Manger JP, Talley EM, Scammell TE, Tonegawa S (2005) Thalamic $Ca_v3.1$ T-type Ca^{2+} channel plays a crucial role in stabilizing sleep. Proc Natl Acad Sci USA 102:1743–1748.

Araya R, Jiang J, Eisenthal KB, Yuste R (2006) The spine neck filters membrane potentials. Proc Natl Acad Sci USA 103:17961–17966.

Batchelor AM, Garthwaite J (1997) Frequency detection and temporally dispersed synaptic signal association through a metabotropic glutamate receptor pathway. Nature 385:74–77.

Batchelor AM, Knöpfel T, Gasparini F, Garthwaite J (1997) Pharmacological characterization of synaptic transmission through mGluRs in rat cerebellar slices. Neuropharmacology 36:401–403.

Baude A, Nusser Z, Roberts JD, Mulvihill E, McIlhinney RA, Somogyi P (1993) The metabotropic glutamate receptor (mGluR1 alpha) is concentrated at perisynaptic membrane of neuronal subpopulations as detected by immunogold reaction. Neuron 11:771–787.

Bloodgood BL, Sabatini BL (2005) Neuronal activity regulates diffusion across the neck of dendritic spines. Science 310:866–869.

Bourinet E, Alloui A, Monteil A, Barrère C, Couette B, Poirot O, Pages A, McRory J, Snutch TP, Eschalier A, Nargeot J (2005) Silencing of the $Ca_v3.2$ T-type calcium channel gene in sensory neurons demonstrates its major role in nociception. EMBO J 24:315–324.

Canepari M, Ogden D (2003) Evidence for protein tyrosine phosphatase, tyrosine kinase, and G-protein regulation of the parallel fiber metabotropic slow EPSC of rat cerebellar Purkinje neurons. J Neurosci 23:4066–4071.

Canepari M, Auger C, Ogden D (2004) Ca^{2+} ion permeability and single-channel properties of the metabotropic slow EPSC of rat Purkinje neurons. J Neurosci 24:3563–3573.

Carter AG, Sabatini BL (2004) State-dependent calcium signaling in dendritic spines of striatal medium spiny neurons. Neuron 44:483–493.

Chadderton P, Margrie TW, Häusser M (2004) Integration of quanta in cerebellar granule cells during sensory processing. Nature 428:856–860.

Chen CC, Lamping KG, Nuno DW, Barresi R, Prouty SJ, Lavoie JL, Cribbs LL, England SK, Sigmund CD, Weiss RM, Williamson RA, Hill JA, Campbell KP (2003) Abnormal coronary function in mice deficient in $alpha_{1H}$ T-type Ca^{2+} channels. Science 302:1416–1418.

Conquet F, Bashir ZI, Davies CH, Daniel H, Ferraguti F, Bordi F, Franz-Bacon K, Reggiani A, Matarese V, Condé F (1994) Motor deficit and impairment of synaptic plasticity in mice lacking mGluR1. Nature 372:237–243.

Crepel F, Daniel H (2007) Developmental changes in agonist-induced retrograde signaling at parallel fiber-Purkinje cell synapses: role of calcium-induced calcium release. J Neurophysiol 98:2550–2565.

Denk W, Sugimori M, Llinás R (1995) Two types of calcium response limited to single spines in cerebellar Purkinje cells. Proc Natl Acad Sci USA 92:8279–8282.

Fahlman CS, Bickler PE, Sullivan B, Gregory GA (2002) Activation of the neuroprotective ERK signaling pathway by fructose-1,6-bisphosphate during hypoxia involves intracellular Ca^{2+} and phospholipase C. Brain Res 958:43–51.

Finch EA, Augustine GJ (1998) Local calcium signalling by inositol-1,4,5-trisphosphate in Purkinje cell dendrites. Nature 396:753–756.

Fritschy JM, Weinmann O, Wenzel A, Benke D (1998) Synapse-specific localization of NMDA and GABA(A) receptor subunits revealed by antigen-retrieval immunohistochemistry. J Comp Neurol 390:194–210.

Hartmann J, Dragicevic E, Adelsberger H, Henning HA, Sumser M, Abramowitz J, Blum R, Dietrich A, Freichel M, Flockerzi V, Birnbaumer L, Konnerth A (2008) TRPC3 channels are required for synaptic transmission and motor coordination. Neuron 59:392–398.

Hildebrand ME, David LS, Hamid J, Mulatz K, Garcia E, Zamponi GW, Snutch TP (2007) Selective inhibition of Cav3.3 T-type calcium channels by Galphaq/11-coupled muscarinic acetylcholine receptors. J Biol Chem 282:21043–21055.

Horowitz LF, Hirdes W, Suh BC, Hilgemann DW, Mackie K, Hille B (2005) Phospholipase C in living cells: activation, inhibition, Ca^{2+} requirement, and regulation of M current. J Gen Physiol 126:243–262.

Ichise T, Kano M, Hashimoto K, Yanagihara D, Nakao K, Shigemoto R, Katsuki M, Aiba A (2000) mGluR1 in cerebellar Purkinje cells essential for long-term depression, synapse elimination, and motor coordination. Science 288:1832–1835.

Iftinca M, Hamid J, Chen L, Varela D, Tadayonnejad R, Altier C, Turner RW, Zamponi GW (2007) Regulation of T-type calcium channels by Rho-associated kinase. Nat Neurosci 10:854–860.

Isope P, Barbour B (2002) Properties of unitary granule cell–>Purkinje cell synapses in adult rat cerebellar slices. J Neurosci 22:9668–9678.

Isope P, Murphy TH (2005) Low threshold calcium currents in rat cerebellar Purkinje cell dendritic spines are mediated by T-type calcium channels. J Physiol 562:257–269.

Izumi Y, Zarrin AR, Zorumski CF (2000) Arachidonic acid rescues hippocampal long-term potentiation blocked by group I metabotropic glutamate receptor antagonists. Neuroscience 100:485–491.

Joksovic PM, Nelson MT, Jevtovic-Todorovic V, Patel MK, Perez-Reyes E, Campbell KP, Chen CC, Todorovic SM (2006) CaV3.2 is the major molecular substrate for redox regulation of T-type Ca^{2+} channels in the rat and mouse thalamus. J Physiol 574:415–430.

Jörntell H, Ekerot CF (2006) Properties of somatosensory synaptic integration in cerebellar granule cells *in vivo*. J Neurosci 26:11786–11797.

Kim D, Song I, Keum S, Lee T, Jeong MJ, Kim SS, McEnery MW, Shin HS (2001) Lack of the burst firing of thalamocortical relay neurons and resistance to absence seizures in mice lacking alpha(1G) T-type Ca^{2+} channels. Neuron 31:35–45.

Kim SJ, Kim YS, Yuan JP, Petralia RS, Worley PF, Linden DJ (2003) Activation of the TRPC1 cation channel by metabotropic glutamate receptor mGluR1. Nature 426:285–291.

Knöpfel T (2007) Two new non-competitive mGlu1 receptor antagonists are potent tools to unravel functions of this mGlu receptor subtype. Br J Pharmacol 151:723–724.

Knöpfel T, Grandes P (2002) Metabotropic glutamate receptors in the cerebellum with a focus on their function in Purkinje cells. Cerebellum 1:19–26.

Lee JH, Gomora JC, Cribbs LL, Perez-Reyes E (1999) Nickel block of three cloned T-type calcium channels: low concentrations selectively block alpha1H. Biophys J 77:3034–3042.

Li L, Bischofberger J, Jonas P (2007) Differential gating and recruitment of P/Q-, N-, and R-type Ca^{2+} channels in hippocampal mossy fiber boutons. J Neurosci 27:13420–13429.

Maejima T, Oka S, Hashimotodani Y, Ohno-Shosaku T, Aiba A, Wu D, Waku K, Sugiura T, Kano M (2005) Synaptically driven endocannabinoid release requires Ca^{2+}-assisted metabotropic glutamate receptor subtype 1 to phospholipase Cβ4 signaling cascade in the cerebellum. J Neurosci 25:6826–6835.

McKay BE, McRory JE, Molineux ML, Hamid J, Snutch TP, Zamponi GW, Turner RW (2006) Ca(V)3 T-type calcium channel isoforms differentially distribute to somatic and dendritic compartments in rat central neurons. Eur J Neurosci 24:2581–2594.

Meacham CA, White LD, Barone S Jr, Shafer TJ (2003) Ontogeny of voltage-sensitive calcium channel alpha(1A) and alpha(1E) subunit expression and synaptic function in rat central nervous system. Brain Res Dev Brain Res 142:47–65.

Middleton SJ, Racca C, Cunningham MO, Traub RD, Monyer H, Knöpfel T, Schofield IS, Jenkins A, Whittington MA (2008) High-frequency network oscillations in cerebellar cortex. Neuron 58:763–774.

Molineux ML, McRory JE, McKay BE, Hamid J, Mehaffey WH, Rehak R, Snutch TP, Zamponi GW, Turner RW (2006) Specific T-type calcium channel isoforms are associated with distinct burst phenotypes in deep cerebellar nuclear neurons. Proc Natl Acad Sci USA 103:5555–5560.

Mouginot D, Bossu JL, Gähwiler BH (1997) Low-threshold Ca2+ currents in dendritic recordings from Purkinje cells in rat cerebellar slice cultures. J Neurosci 17:160–170.

Otsu Y, Bormuth V, Wong J, Mathieu B, Dugue GP, Feltz A, Dieudonne S (2008) Optical monitoring of neuronal activity at high frame rate with a digital random-access multiphoton (RAMP) microscope. J Neurosci Methods 173:259–270.

Ottersen OP, Landsend AS (1997) Organization of glutamate receptors at the synapse. Eur J Neurosci 9:2219–2224.

Pereverzev A, Mikhna M, Vajna R, Gissel C, Henry M, Weiergräber M, Hescheler J, Smyth N, Schneider T (2002) Disturbances in glucose-tolerance, insulin-release, and stress-induced hyperglycemia upon disruption of the Ca(v)2.3 (alpha 1E) subunit of voltage-gated Ca^{2+} channels. Mol Endocrinol 16:884–895.

Perez-Reyes E (2003) Molecular physiology of low-voltage-activated t-type calcium channels. Physiol Rev 83:117–161.

Petrenko AB, Tsujita M, Kohno T, Sakimura K, Baba H (2007) Mutation of alpha1G T-type calcium channels in mice does not change anesthetic requirements for loss of the righting reflex and minimum alveolar concentration but delays the onset of anesthetic induction. Anesthesiology 106:1177–1185.

Pouille F, Cavelier P, Desplantez T, Beekenkamp H, Craig PJ, Beattie RE, Volsen SG, Bossu JL (2000) Dendro-somatic distribution of calcium-mediated electrogenesis in Purkinje cells from rat cerebellar slice cultures. J Physiol 527:265–282.

Rancz EA, Häusser M (2006) Dendritic calcium spikes are tunable triggers of cannabinoid release and short-term synaptic plasticity in cerebellar Purkinje neurons. J Neurosci 26:5428–5437.

Rancz EA, Häusser M (2007) Somatic firing hyperpolarizes Purkinje cell dendrites. Soc Neurosci Abstr 33:251.10.

Roth A, Häusser M (2001) Compartmental models of rat cerebellar Purkinje cells based on simultaneous somatic and dendritic patch-clamp recordings. J Physiol 535:445–472.

Sacco T, Tempia F (2002) A-type potassium currents active at subthreshold potentials in mouse cerebellar Purkinje cells. J Physiol 543:505–520.

Shigemoto R, Nakanishi S, Mizuno N (1992) Distribution of the mRNA for a metabotropic glutamate receptor (mGluR1) in the central nervous system: an in situ hybridization study in adult and developing rat. J Comp Neurol 322:121–135.

Shin J, Shen F, Huguenard J (2007) PKC and polyamine modulation of GluR2-deficient AMPA receptors in immature neocortical pyramidal neurons of the rat. J Physiol 581:679–691.

Soong TW, Stea A, Hodson CD, Dubel SJ, Vincent SR, Snutch TP (1993) Structure and functional expression of a member of the low voltage-activated calcium channel family. Science 260:1133–1136.

Staub C, Vranesic I, Knöpfel T (1992) Responses to metabotropic glutamate receptor activation in cerebellar Purkinje cells: induction of an inward current. Eur J Neurosci 4:832–839.

Svoboda K, Tank DW, Denk W (1996) Direct measurement of coupling between dendritic spines and shafts. Science 272:716–719.

Swensen AM, Bean BP (2003) Ionic mechanisms of burst firing in dissociated Purkinje neurons. J Neurosci 23:9650–9663.

Tai C, Kuzmiski JB, MacVicar BA (2006) Muscarinic enhancement of R-type calcium currents in hippocampal CA1 pyramidal neurons. J Neurosci 26:6249–6258.

Takechi H, Eilers J, Konnerth A (1998) A new class of synaptic response involving calcium release in dendritic spines. Nature 396:757–760.

Talley EM, Cribbs LL, Lee JH, Daud A, Perez-Reyes E, Bayliss DA (1999) Differential distribution of three members of a gene family encoding low voltage-activated (T-type) calcium channels. J Neurosci 19:1895–1911.

Tanaka J, Nakagawa S, Kushiya E, Yamasaki M, Fukaya M, Iwanaga T, Simon MI, Sakimura K, Kano M, Watanabe M (2000) Gq protein alpha subunits Galphaq and Galpha11 are localized at postsynaptic extra-junctional membrane of cerebellar Purkinje cells and hippocampal pyramidal cells. Eur J Neurosci 12:781–792.

Tempia F, Alojado ME, Strata P, Knöpfel T (2001) Characterization of the mGluR(1)-mediated electrical and calcium signaling in Purkinje cells of mouse cerebellar slices. J Neurophysiol 86:1389–1397.

Topolnik L, Azzi M, Morin F, Kougioumoutzakis A, Lacaille JC (2006)

mGluR1/5 subtype-specific calcium signalling and induction of long-term potentiation in rat hippocampal oriens/alveus interneurones. J Physiol 575:115–131.

Tsuruno S, Kawaguchi SY, Hirano T (2008) Src-family protein tyrosine kinase negatively regulates cerebellar long-term depression. Neurosci Res 61:329–332.

Wang SS, Denk W, Häusser M (2000) Coincidence detection in single dendritic spines mediated by calcium release. Nat Neurosci 3:1266–1273.

Watanabe S, Takagi H, Miyasho T, Inoue M, Kirino Y, Kudo Y, Miyakawa H (1998) Differential roles of two types of voltage-gated Ca2+ channels in the dendrites of rat cerebellar Purkinje neurons. Brain Res 791:43–55.

Welsby PJ, Wang H, Wolfe JT, Colbran RJ, Johnson ML, Barrett PQ (2003) A mechanism for the direct regulation of T-type calcium channels by Ca^{2+}/calmodulin-dependent kinase II. J Neurosci 23:10116–10121.

Wolfe JT, Wang H, Howard J, Garrison JC, Barrett PQ (2003) T-type calcium channel regulation by specific G-protein betagamma subunits. Nature 424:209–213.

Womack MD, Khodakhah K (2004) Dendritic control of spontaneous bursting in cerebellar Purkinje cells. J Neurosci 24:3511–3521.

Yuan Q, Qiu DL, Weber JT, Hansel C, Knöpfel T (2007) Climbing fiber-triggered metabotropic slow potentials enhance dendritic calcium transients and simple spike firing in cerebellar Purkinje cells. Mol Cell Neurosci 35:596–603.

Zamponi GW, Bourinet E, Snutch TP (1996) Nickel block of a family of neuronal calcium channels: subtype- and subunit-dependent action at multiple sites. J Membr Biol 151:77–90.